TÜRKİYE
FIRAT UNIVERSITY
GRADUATE SCHOOL OF NATURAL AND APPLIED SCIENCES

ON DETERMINATION OF SOIL RADON-222 GAS, METEOROLOGICAL PARAMETERS, ATMOSPHERIC TOTAL ELECTRON CONTENT AND POSSIBLE RELATIONSHIPS BETWEEN EARTHQUAKES: A MONTE CARLO FORECASTING SIMULATION APPLICATION

Mustafa Khairi ARAB

Master's Thesis

DEPARTMENT OF PHYSICS

Division of Nuclear Physics

JUNE 2020

TÜRKİYE
FIRAT UNIVERSITY
GRADUATE SCHOOL OF NATURAL AND APPLIED SCIENCES

Department of Physics

Master's Thesis

ON DETERMINATION OF SOIL RADON-222 GAS, METEOROLOGICAL PARAMETERS, ATMOSPHERIC TOTAL ELECTRON CONTENT AND POSSIBLE RELATIONSHIPS BETWEEN EARTHQUAKES: A MONTE CARLO FORECASTING SIMULATION APPLICATION

Author
Mustafa Khairi ARAB

Supervisor
Prof. Dr. Fatih KÜLAHCI

JUNE 2020
ELAZIG

TÜRKİYE
FIRAT UNIVERSITY
GRADUATE SCHOOL OF NATURAL AND APPLIED SCIENCES

Department of Physics

Master's Thesis

Title:	On Determination of Soil Radon-222 Gas, Meteorological Parameters, Atmospheric Total Electron Content and Possible Relationships Between Earthquakes: A Monte Carlo Forecasting Simulation Application
Author:	Mustafa Khairi ARAB
Submission Date:	1 June 2020
Defense Date:	16 June 2020

THESIS APPROVAL

This thesis, which was prepared according to the thesis writing rules of the Graduate School of Natural and Applied Sciences, Fırat University, was evaluated by the committee members who have signed the following signatures and was unanimously approved after the defense exam made open to the academic audience.

		Signature
Supervisor:	Prof. Dr. Fatih KÜLAHCI Firat University, Faculty of Science	Approved
Chair:	Title Name SURNAME ... University, Faculty of	Approved
Member:	Title Name SURNAME ... University, Faculty of	Approved
Member:	Title Name SURNAME ... University, Faculty of	Approved
Member:	Title Name SURNAME ... University, Faculty of	Approved
Member:	Title Name SURNAME ... University, Faculty of	Approved

This thesis was approved by the Administrative Board of the Graduate School on
01 / 06 / 2020

Signature

Prof. Dr. Soner ÖZGEN
Director of the Graduate School

DECLARATION

I hereby declare that I wrote this Master's Thesis titled “On Determination of Soil Radon-222 Gas, Meteorological Parameters, Atmospheric Total Electron Content and Possible Relationships Between Earthquakes: A Monte Carlo Forecasting Simulation Application” in consistent with the thesis writing guide of the Graduate School of Natural and Applied Sciences, Firat University. I also declare that all information in it is correct, that I acted according to scientific ethics in producing and presenting the findings, cited all the references I used, express all institutions or organizations or persons who supported the thesis financially. I have never used the data and information I provide here in order to get a degree in any way.

16 June 2020

Mustafa Khairi ARAB

PREFACE

Although this thesis is a master's thesis, it includes many innovations in its field. Many studies can be found in the literature about earthquakes and atmospheric electron content and also the change of earthquakes with soil radon concentrations. However, there is no research in the literature on earthquake-radon-TEC trilogy. On the other hand, these innovations were not satisfied, and the variables were modeled with Monte Carlo Simulation. Thanks to this modeling, the estimation of the quantities of the relevant variables has also been made for forward time periods. In this regard, the research contains an important originality.

I would like to give a warm thank to my supervisor for his advices and patient and colleague Ahmed Mohammed who have helped improve this thesis.

Mustafa Khairi ARAB
ELAZIG, 2020

TABLE OF CONTENTS

ABSTRACT

On Determination of Soil Radon-222 Gas, Meteorological Parameters, Atmospheric Total Electron Content and Possible Relationships Between Earthquakes: A Monte Carlo Forecasting Simulation Application

Mustafa Khairi ARAB

Master's Thesis

FIRAT UNIVERSITY
Graduate School of Natural and Applied Sciences

Department of Physics

June 2020, Page: xii + 66

In the literature, no research is available on determining the relationship between earthquakes and Total Electron Content (TEC) and Radon-222 gas concentrations. One of the main reasons for this study is to take an important step to close the gap mentioned in this field. In this area, there are studies on the change of TEC in the atmosphere close to the ground and the relationship between earthquakes and researches on Rn-222 and earthquake co-exchange. However, no research has yet been conducted where three of these changes are together. In this study, Erzincan-Ekşisu, a seismically highly active region on the North Anatolian Fault Line, was chosen as the research area. The statistical distributions of the data obtained were determined and modelled using ARIMA and Monte Carlo Simulation techniques and predictions were made for future data estimates.

Keywords: Earthquakes, Time series, Monte Carlo, ARIMA, MATLAB

ÖZET

Toprak Radon-222 Gazı, Meteorolojik Parametreler, Atmosferik Toplam Elektron İçeriği ve Depremler Arasındaki Olası İlişkilerin Belirlenmesi Üzerine: Bir Monte Carlo Tahmin Simülasyon Uygulaması

Mustafa Khairi ARAB

Yüksek Lisans Tezi

FIRAT ÜNİVERSİTESİ
Fen Bilimleri Enstitüsü

Fizik Anabilim Dalı
Nükleer Fizik
Haziran 2020, Sayfa: xii + 66

Literatürde, depremlerin Toplam Elektron İçeriği (TEC) ile Radon-222 gaz konsantrasyonları ile ilişkisinin belirlenmesi üzerine hiç bir araştırma mevcut değildir. Bu çalışmanın yapılmasının temel nedenlerinden birisi, bu alanda bahsedilen eksiği kapatmak için önemli bir adım atmaktır. Bu alanda yere yakın atmosferdeki TEC'in değişimi ve depremlerin ilişkisi üzerine çalışmalar ve yine Rn-222 ve depremlerin birlikte değişimi üzerine araştırmalar vardır. Fakat bu değişimlerin, üçünün birlikte olduğu bir araştırma henüz yapılmamıştır. Bu çalışmada, araştırma alanı olarak Kuzey Anadolu Fay Hattı üzerinde bulunan ve sismik olarak oldukça aktif bir bölge olan Erzincan-Ekşisu seçildi. Elde edilen verilerin istatistiksel dağılımları belirlendi ve ARIMA ve Monte Carlo Simülasyon teknikleri kullanılarak modellendi ve ileriye dönük veri tahminleri için öngörüler yapıldı.

Anahtar Kelimeler: Depremler, Zaman serileri, Monte Carlo, ARIMA, MATLAB

LIST OF FIGURES

Page

LIST OF TABLES

Page

LIST OF APPENDICES

Page

SYMBOLS AND ABBREVIATIONS

Symbols

Km/hr	: Kilometer per Hours
t1/2	: Half- life
hrs	: Hours
km2	: KiloMeter Square
%	: Percentage
µSv	: Micro siviert
Km	: KiloMeter
°C	: Celezi
Ω	: Ohm's
Rc	: Columnar resistance
Cc	: Capacitance of this circuit

Abbreviations

ACF	: Autocorrelation function
AIC	: Akaike Information Criterion
AR	: Autoregressive
ARIMA	: Auto Regressive integrate moving Average
BIC	: Bayesian Information Criterion
Bqkg−1	: Becquerel per Kilogram
Bqm-2	: Becquerel per meter square
Bqm-3	: Becquerel per meter cube
cm	: Centimeter
DNA	: Deoxyribo nucleic acid
EAFZ	: East Anatolian Fault Zone
I	: Integrated
IAEA	: International atomic energy Agency
ICME	: Integrated computational materials engineering
kBqm-3	: Kilobecqurerel per meter cube
m	: Meter
MA	: Moving Average
mBqm−2 h−1	: MilliBecquerel per metersquare hour
min	: Minute
ML	: Local Magnitude
mSvy-1	: Millisievert per hours
NAF	: North Anatolian Fault
NAFZ	: North Anatolian Fault Zone
NORM	: Natural occurring radioactive material
PACF	: Partial Autocorrelation Function
Rn	: Radon
SSNTD	: Solid State nuclear Track Detector
TEC	: Total electron content
TECU	: Total electron content Unit
NCRP	: National Council on Radiation Protection and Measurements
GEC	: Global electric circuit

1. INTRODUCTION

An overview of the radioactivity, specifically ^{222}Rn isotope is related to the prediction of the earthquakes in some of most active seismically continental strike-slip fault zones. Also the effects of some metrological parameters and atmospheric total electron content TEC on earthquakes will be clarified.

1.1. Environmental Radiation Background

The nature of the earth planet consists of above 60 radionuclides or radioelements. These radionuclides can be classified in general to three groups; first, the primordial radionuclides which are existed during the formation of the universe. Second, Cosmogenic radionuclides that formed by interaction of cosmic ray with atmospheric atoms and molecules. Third, radionuclides that produced wither accidently or in purpose by human actions. Even though, this group represents minor quantity compared to the other two [1].

Naturally Occurring Radioactive Materials (NORM) is those radionuclides naturally placed in the earth crust. With the time they distributed by varying amounts in soil, rocks air, water, plants, and consequently in humans and animals. Generally speaking, they are present throughout our ecosystem [2, 3].

Due to the erosion process and solubility of NORM radionuclides and their decay progenies, most of these are transported from earth crust into ground and surface water. Uranium and thorium for instance are found in ground and surface waters due to its natural occurrence in geological formations. Accordingly, radionuclides in the surface soil and those in the water (ground and surface water) may transfer to the food chain through planting and irrigation waters, even directly to human from the water supply [2].

The environmental background of natural radiation arises mainly from terrestrial and secondly from cosmic sources. The sources of cosmic rays are high-energy protons and charged nuclei originated from solar and other galaxies. These high-energy particles bombard and interact with stable atoms and molecules present in the upper earth atmosphere constantly. Accordingly, cosmic rays cause direct human exposure and secondary exposure from the produced radionuclides. The exposure occurs by inhalation and/or by ingestion after their uptake by plants or by skin uptake [3]. Some of these spreader radionuclides produced by cosmic rays in the atmosphere (^{7}Be, ^{14}C, ^{32}Si, ^{26}Al and ^{36}Cl) contribute a measurable dose to humans about 12 μSv annually [4].

In the radio ecological context, the long lived fission products radioisotope of 137Cs are among the most hazardous radionuclides being released into the biosphere following weapons tests in the 1950's and 1960's. A significant amount of nuclear fission products fallout from nuclear reactor accidents of Chernobyl in 1986 and Fukushima in 2011 contaminated wide areas all over the world [5].

As all studies confirmed that the estimation of external dose caused by gamma ray from natural radionuclides sources is exceptionally the higher among other radiation sources. The earth crust is the main source of natural radionuclides such as the heavy isotopes ^{235}U, ^{238}U, ^{232}Th and their chains radionuclides, in addition to a single primordial radioisotope ^{40}K. The densities of the above radionuclides differ from one region to another of the earth crust all over the world depending on the local geological formation of that region. Therefore, the exposure doses from these natural radionuclides are also varied as it depends on their concentrations in the soil and rocks [6].

One of the main and most popular radioactive radionuclide besides Uranium and thorium in the 19th and 20th centuries is the radon isotope. It represents another major exposure pathway to natural radiation. Since its discovery (in the 18th century), radon has widely been studied and its applications can be found in a variety of fields such as Seismic studies, atmospheric physics as well as in nuclear physics. It is well known that ^{238}U and all its daughters are in a solid state, but ^{222}Rn, formed from the decay of ^{226}Ra, in a gaseous state. Therefore, only ^{222}Rn can transfer into the atmosphere through soil, surface water and building materials emanations. According to the very low half-life t1/2 = 3.8 days of ^{222}Rn is enough to allow it and its progenies to contaminate atmospheric air effectively near the ground. Due to its successive decays and most of its daughters (^{218}Po, ^{214}Pb, ^{214}Bi and ^{214}Po) decay by alpha particles, they become the main sources of internal exposure by inhalation and causing lung cancer. The rapidly decaying of ^{222}Rn and its successive progenies become a leading part of total radiation background, which roughly represent about 55% of the total background [4].

Even though the radium ^{226}Ra concentration in earth crust soil and rocks is nearly constant in each geological form, the ^{222}Rn concentration as gas in soil varied as a function of regional factors such as geophysical, hydrogeological, geochemical phenomena (earthquakes, volcanic etc.). It is well known that the weather conditions such as rain precipitation, wind velocity, pressure and temperature have greater effects on surface soil than the deeper parts. Accordingly, the ^{222}Rn migration is strongly affected by these metrological factors [7].

The important of radon gas is coming from its physical properties. It exists in nature as radioactive isotopes of short half-life. Radon gas is lighter than air which makes it diffuse through the earth crust and rises in the air until it is completely decayed. Once radon gas introduced into the air it and its radioactive daughter's decays pose a great risk to human health due to fast energy releasing in the forms of alpha, beta and γ- rays. Even though this energy released into the air is tiny but very destructive. As alpha particles released represent the common energy released, it is the biggest of the three and is the most destructive. The most health problem is coming from the inhalation of that gas and then decay in human being lungs with an outcome of lung cancer. It is believed that cancer needs at least one mutation and then the proliferation of intermediate cells that have undergone some degree of DNA damage. Damage to DNA can occur at any exposure level [8].

Environmental pollution in a time being is considered as an important subject for debate or to be searched internationally at all scientific and humanism levels, even political. A lot of conferences have been systematically organized all over the world to find out some solutions to this problem. The environmental health risks that affect our nature and our lives due to natural radioactivity and that resulting from human activities have turn into a significant issue in this century. Since the formation of the International Atomic Energy Agency (IAEA) in 1957, global cooperation has been in the peaceful use of nuclear power whether via production of electric energy from nuclear power plant or application activities on radioactive sources have played an important role in global development. [9].

Earth's atmosphere layers up to ionosphere constitute different chemical compositions. Different investigations approved the relationship of the atmospheric electric field with radioactivity. Many efforts have been carried out to understand earthquakes and how to employment the change of atmospheric electric field and conductivity to predict earthquake before it strikes. Also the Total Electron Content (TEC) is an essential descriptive quantity for the earth's ionosphere. Even though TEC and atmospheric electric field are affected tremendously by some other earth's natural phenomena such as climate change, they are still favourite parameters under investigation to monitor for possible space weather impacts [10].

In order of coupling the anomalies of radon concentration with the vertical atmospheric electric field the study must cover some available resources for earth surface soil and water radon gas. Such coupling has been carried out in near ground atmosphere up to the ionosphere in some seismically active areas. Despite tremendous efforts, still the relationship between radon emanation and seismicity is not well understood, but more significant milestones should be achieved; therefore, in this work, a survey study of the relationship between atmospheric electric field and total electron density as another variable has been conducted.

1.2. Literature Review

There are many studies carried out all over the world using different detection systems, all according to the type and energy of radiation and of detector appropriate for the study, to knowledge the environmental pollution due to radioactive isotopes. Different investigations of radon gas concentration measurements in soil, water and soil gas in adverse Tectonics and

Geological regions have been carried out in Turkey and all over the world. Some of most important studies by various authors will be reviewed in the following sections.

1.2.1. Local Studies

In the study conducted by M. Kamışlıoğlu and F. Külahci, a nonlinear characteristic of a complex dynamic system behavior of ^{222}Rn gas was examined by correlation dimension techniques [11]. Chaotic time series analyses had been applied on ^{222}Rn concentration of soil data measured every 15-min along January to December of the year 2007. 70272 ^{222}Rn concentration data were taken belong to the regions Kozan and Yakapinar regions close to the East Anatolian Fault Zone (EAFZ) in Turkey. The study approved the nonlinearity and the geometric figure behavior of ^{222}Rn gas and that the chaotic time series results are strongly chaotic properties of seismically active region. In addition, this nonlinear dynamic methodology is sufficient to use to predict earthquakes.

F. Külahci and Ş. Çiçek collected and analyzed concentrations data of radon gas from soil and water for more than eight months of a section of the highest seismically active areas in an entire world located in the East Anatolian Fault Zone of Turkey [12]. Samples were collected from 50-cm depth of the soil surface on the lake shore, while water samples were taken from about 10 m from the shore at 30 cm depth. During the same period, about 110 micro and macro earthquakes had been documented. On 6/23/2011 the largest earthquake in İçme of magnitude ML 5.4 on Richter scale earthquake take place. Just before this largest earthquake by twenty days, irregular increases of ^{222}Rn gas concentrations of soil and water were noticed as analyzed in a time-series. Authors concluded that this might be a good indicator to predict the earthquake. In addition, they recorded an increase of about 70–99 % of ^{222}Rn gas concentrations just a few days before that earthquake. Accordingly, they attributed such anomaly of ^{222}Rn data before the earthquake to the stress accumulation prior to the earthquake.

H. Yakut et.al. recorded and analyzed ^{222}Rn gas concentrations data of soil concerning the west section of the North Anatolian Fault Zone, Turkey [13]. They used Solid State Nuclear Track Detectors (SSNTD) type LR-115 in the borehole of about 50-cm deep of the soil surface at 12 different stations along the fault line for 12 monthly periods. They found an average of 1930 Bqm-2 radon concentration which varied from 29 to 7059 Bqm-2 influence by different meteorological parameters such as a linear relation between mean soil temperature and radon activity and a reverse proportionality of radon level with the rest meteorological parameters such as humidity, pressure and precipitation. Maximum and minimum ^{222}Rn concentrations recorded were in summer and winter seasons respectively.

The 3D seismic velocity model of the upper earth crust under the Erzincan Basin was examined by Mr. Akter et al. [14]. The application of sectional reflection or tomographic inversion on the arrival of the body wave of the earthquake occurred in Erzincan on March 13, 1992 of ML = 6.9 was adopted after a shock sequence. The conclusion reached by the analysis is that the continuation of the northern Anatolia rift extending eastwards might be a branch of the Euphrates Valley, which constitutes the main seismic risk factor.

1.2.2. Foreign Studies

K. Hayashi et.al. They collected data of ^{222}Rn concentration for almost five years from 2003 to 2007 [15]. A comparison between these data and that of the preliminary period of 2008 to the March 2011, the date of Tohoku-Oki Earthquake was carried out. Irregular radon concentration readings of soil-gas have been observed before an earthquake action. They come out, fitting by sinusoidal model, to relate the variation of ^{222}Rn concentrations with seasons. The limit was determined by considering a change in concentrations that are strongly influenced by surface temperature variation and to a lesser extent by with atmospheric turbulence. It has been found that applying the method with getting about 70 days before the event to the change in seasonal data can be applied to identify radon anomalous variation prior the earthquake.

A developed Finite Element numerical model was adopted by (Y. I. Hafez1 and El-S. Awad) to predict the concentration of radon as a function of the earth crust depth, the diffusion coefficients of soil layers, the soil gas radon concentrations and fluxes [16]. Radon data with depth were collected from previous studies of different geophysical locations representing four countries, South Africa, Jordan, Germany, and Greece. This investigation showed the power and flexibility of this numerical method. They also concluded the non-monotonic nature of radon, and that a geophysical parameter is the diffusion coefficient in natural soil. They also confirm radon profile multi-layer behavior at all locations. Finally, ^{222}Rn transfer coefficient from soil to air is proposed to be 0.0002 cm/s.

W. Zhou et.al, suggested a model of two main factors to idealize a prediction of the ^{222}Rn gas flux in soil more accurately and practically [17]. The first variables that control radon transportation in soil are the ^{222}Rn emanation power and the second is the soil water content. The reformulated model was verified for such prediction, which had been done by the site measurements accomplished in 10 different locations of 20 different soil samples as a total (6 of clay, 6 of silt and 8 of sand). The model had been improved to be useful for global information in earthquake prediction feasibility via the accuracy of the earth surface flux density of radon.

H. Mansour measured radon specific activity of 28 indoor homes in Erbil /Iraq during autumn season by a passive radon track dosimeter type CR-39 [18]. The mean concentration of radon found in these homes was 44 ± 23 Bqm-3 and ranged from 10.33-90.34 Bqm-3. These values fall within the world standard level. While the calculated average absorption effective dose, using the values of 0.5 and 0.8 as equilibrium factor and occupancy factor respectively, per person living in home was 1.3 ± 0.65 mSvy-1. The expected average lung cancer/year among each (106) persons was found to be 23 ± 12 cancer case.

An investigation to relate the radon emanation and the variations of the ionosphere parameters in seismically active regions has been conducted by S. A. Pulinets et.al. [19]. Since alpha-particle emitted by ^{222}Rn produce about 2×105 electron-ion pairs then, near the ground atmosphere a huge number of ionizations are produced. Accordingly, creates a quasi-stationary anomalous electric field in this atmosphere which can be assumed to be the main agent of the coupling mechanism between earthquakes and atmosphere then penetrated into the ionosphere. Atmospheric conductivity as a function of the height from the earth surface had been theoretically modeled and compared with some experimental data. From such comparison, they concluded that coupling between radon and monitoring the ionosphere Vertical distribution may act as a powerful tool for earthquake prediction.

1.3. Objective of the Study

The aim behind the present work is not a repetition of what was already done but rather highlighting the important and related parts of the subject of relating ^{222}Rn activity with the prediction of earthquake. In addition this thesis focuses on the analyses of some values of radioactive radon gas concentrations obtained from seismic stations near the tectonically complicated and high seismically active location of Erzincan district, Ekşisu city of North Anatolian Fault (NAF), Turkey. Results from these sites for duration of approximately three years within short measuring periods of up to 15 minutes are considered. ^{222}Rn concentrations are studied according to time series analysis for different periods of 15 minutes. In this study an implementation of the Auto-Regressive Integrated Moving Average (ARIMA) model and Monte-Carlo simulations build in MATLAB package is adopted to analyze the time series of ^{222}Rn data and to see the possible order of combination of auto regression as well as the moving average.

1.4. Outlines of the Study

Finally, the **first chapter** reviews definitions and early research works on the subject of the radon emanation and the variations of the ionosphere parameters in seismically active regions. Also it discusses existing literatures on levels of radon concentration as time series analysis in water and soil gas inside (local) Turkey country and some of the world countries. The remaining chapters of the thesis are devoted as follows:

Chapter Two illustrates the theory behind radioactivity, ^{222}Rn background; properties such as transportation, detection, uses and interaction of radon with atmosphere are given.

Chapter Three statistical analysis of time series and atmospheric electric field using ARIMA and Monte Carlo build in MATLAB code. Atmospheric Total Electron Content, atmospheric plasma, its variability Near-Ground atmospheric layers and radon and seismic signatures in the ionosphere will be discussed. Finally the description of the study area will be given, including the geographical location, climate and land.

Chapter Four is devoted to the implementation of the ARIMA(p,d,q) model and Monte-Carlo simulations, then comparing the outcome analysis with the achieved results.

Chapter Five completes this research with conclusions from the current work and general

2. THEORY

Radon and its applications have widely considered in a variety of fields. Such as, fields of seismic studies, atmospheric physics as well as nuclear physics. Theory behind ^{222}Rn as a volatile radionuclide is still under exploration. Although efforts focus on radon itself, progress in the application of ^{222}Rn that specifically relates to earthquake precursory and the variation atmospheric behaviours must be analysed, and the focus is on the change in electrical field and conductivity of the earth atmosphere, which resulted from radon emission from soil and water to the atmosphere. Many mathematical expressions and models had been created and still in most cases.

2.1. Radioactivity

Radioactivity is the phenomenon of the spontaneous decay and transformation of unstable nucleus of atoms with nuclear particle emission and electromagnetic radiation. The three main types of radiation are α-rays (helium nuclei with only 2 protons and two neutrons), β-rays (electrons or positron), and γ-rays (photons).

The concentration or activity of radioisotope source is defined as the rate of radioactive decay of that isotope and is given by the fundamental law of radioactivity [20].

$$C = -\frac{dN}{dt} = \lambda N \tag{2.1}$$

Where *N is* the number of nuclei or atoms of the radionuclide at time *t*, λ is the decay constant, and *A* is an activity expressed in disintegrations per second.

SI special unit for the activity is the Becquerel (1Bq = 1dis/sec), and the standard unit of activity is the curie (1Curie = 3.7×10^{10} Bq). By integration of Equation 2-1 for the time *t*=0 to *t*, the number of radioactive atoms N_0 change to *N* [21].

$$N = N_0 e^{-\lambda t} \tag{2.2}$$

The radioactive half-life, which is defined as the amount of time needed to decrease the activity to half its original value, $N=N_0/2$.

$$t_{1/2} = \frac{0.693}{\lambda} \tag{2.3}$$

Chain decay is the task of nuclear transformation where a radionuclide successively decays to a stable nuclide through a series of radio-nuclides. Look up the case of a triple chain for simplicity [20].

$$N_1 \xrightarrow{\lambda_1} N_2 \xrightarrow{\lambda_2} N_3 \quad stable$$

here λ_1 and λ_2 are the decay constants of (N_1) as a parent and (N_2) as daughter, respectively.

The decay equations are as follows:

$$\frac{dN_1(t)}{dt} = -\lambda_1 N_1(t) \qquad (a)$$
$$\frac{dN_2(t)}{dt} = \lambda_1 N_1(t) - \lambda_2 N_2(t) \qquad (b) \qquad (2.4)$$
$$\frac{dN_3(t)}{dt} = -\lambda_2 N_2(t) \qquad (c)$$

The number of N1 atoms

The details of this system of equations' solution depend on the initial condition; the general case is when number of atoms of the three nuclides at the time (t=0) have N_{10}, N_{20}, N_{30} atoms. N_1 as a function of time can be immediately written down.

$$N_1 = N_{10} e^{-\lambda_1 t} \qquad (2.5)$$

And the numbers of nuclides of other two nuclides are:

$$N_2 = N_{10} \frac{\lambda_1}{\lambda_2 - \lambda_1} (e^{-\lambda_1 t} - e^{-\lambda_2 t}) + N_{20} e^{-\lambda_2 t} \qquad (2.6)$$

$$N_3 = N_{10} \frac{\lambda_1 \lambda_2}{\lambda_2 - \lambda_1} \left\{ \frac{1 - e^{-\lambda_1 t}}{\lambda_1} - \frac{1 - e^{-\lambda_2 t}}{\lambda_2} \right\} + N_{20}(1 - e^{-\lambda_2 t}) + N_{30} \qquad (2.7)$$

By beginning the decay of the chain, the quantity of the parent nuclide decreases with time, while successive daughters increase in different fashions with time. We may have the following three scenarios depending on the values of the constants of decay.

1) If $\lambda_1 > \lambda_2$, the short-lived parent compared to the daughter, then after a long time $t >> 1/\lambda_1$, Equation 2.6 becomes:

$$N_2 = N_{10} \frac{\lambda_1}{\lambda_1 - \lambda_2} e^{-\lambda_2 t} \qquad (2.8)$$

As shown in Figure 2.1(a), there is no equilibrium.

2) If $\lambda_1 < \lambda_2$, the long-lived parent compared to the daughter, then after long time $t >> 1/\lambda_2$, the second exponential can be neglect in Equation 2.6 to get;

$$N_2 \approx N_{10} \frac{\lambda_1}{\lambda_2 - \lambda_1} e^{-\lambda_1 t} \qquad (2.9)$$

$$\frac{A_2}{A_1} = \frac{\lambda_2 N_2}{\lambda_1 N_1} \approx \frac{\lambda_2}{\lambda_2 - \lambda_1} \qquad (2.10)$$

This case is known as transient equilibrium, as shown in Figure 2.1(b)

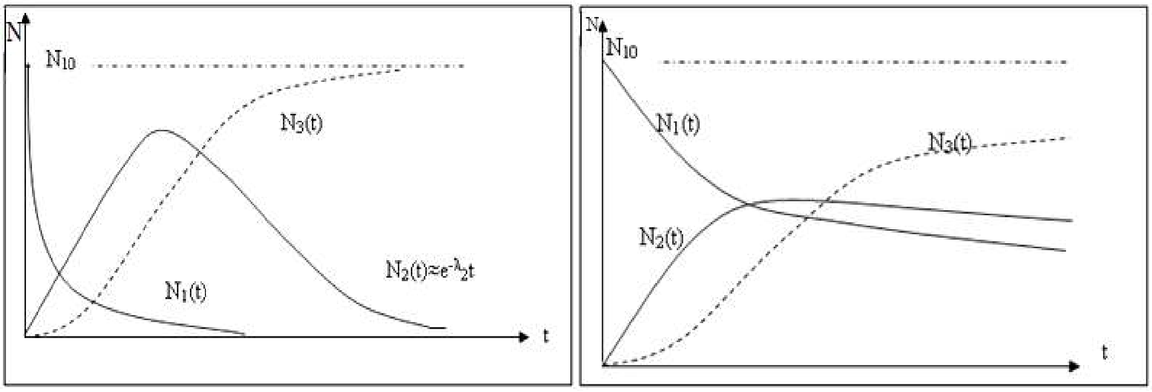

(a) (b)

Figure 2.1. Decay of a radioactive daughter (a) Short-lived parent. (b) Long-lived parent (transient equilibrium) [20]

3) If $\lambda_1 << \lambda_2$, the parent half-life is much greater than the half-life of the daughter, and consequently, the activities of all nuclides are equal [23].

$$\lambda_1 N_1 = \lambda_2 N_2 \quad or \quad C_1 = C_2 \tag{2.11}$$

In this case, we reach what we call secular equilibrium, which is the case of primordial radionuclides ^{238}U, ^{232}Th, as shown in Figure 2.2.

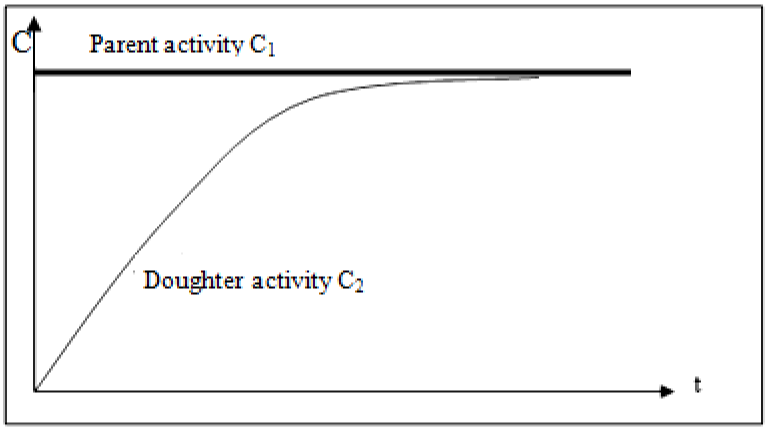

Figure 2.2. Secular equilibrium activity curve as λ1 ≈ 0 [20]

Equations.2.5, 2.6, and 2.7 are known as the Bateman equations. Now, using Equation 2.1 to convert number of atoms of the radionuclide at time *N(t)* to activity *C*, the Bateman's equations given in terms of recurrence relations by Jenkins (2002) were used to model the concentration or specific activity (C) in air for a given nuclide in the radon decay chain, Figure 2.3b. as a function of decay constant λ and time t as follows [22];

$$C_1 = C_{1,0} f_{11} \tag{2.12}$$

$$C_2 = C_{1,0} \lambda_2 f_{12} + C_{2,0} f_{22} \tag{2.13}$$

$$C_3 = C_{1,0} \lambda_2 \lambda_3 f_{13} + C_{2,0} \lambda_3 f_{23} + C_{3,0} f_{33} \tag{2.14}$$

$$C_4 = C_{1,0} \lambda_2 \lambda_3 \lambda_4 f_{14} + C_{2,0} \lambda_3 \lambda_4 f_{24} + C_{3,0} \lambda_4 f_{34} + C_{4,0} f_{34} \tag{2.15}$$

Where C_1, C_2, C_3 and C_4 are respectively the activities of ^{222}Rn, ^{218}Po, ^{214}Pb, and ^{214}Bi to be determined in Bqm^{-3}, $C_{1,0}$, $C_{2,0}$, $C_{3,0}$ and $C_{4,0}$ are the initial concentration of ^{222}Rn, ^{214}Pb, ^{214}Bi and ^{210}Pb (in Bqm^{-3}). The values λ_1, λ_2, λ_3 and λ_4 (s^{-1}) are respectively the decay constants for ^{222}Rn, ^{214}Po, ^{214}Bi and ^{210}Pb, whereas the radioactive decay of each radionuclide f_{ii} is given by $f_{ii} = exp$ ($\lambda_i t$) and the factors f_{ij} are defined for the decay of initially present radionuclide i to the subsequent radionuclide j.

$$f_{ij} = \frac{f_{ii} - f_{jj}}{\lambda_j - \lambda_i} \tag{2.16}$$

Here two assumptions are considered, refer to Figure 2.3b. First ^{222}Rn decays directly to ^{214}Pb by emitting two alphas of decay energy 11.71MeV bypassing ^{218}Po due to its relative short half-life. Second in a similar way assuming a direct decay of ^{214}Pb to ^{210}Pb releasing the sum of one alpha and one beta particle of energy 11.15MeV., in the meanwhile ignoring the decay of ^{210}Pb since it accurse very slowly mostly in the soil subsurface not in the atmosphere with a very low energy (0.064 MeV) which can be neglected [23].

2.2. Radon Studies

Radon has attracted the attention of scholars, and its study became interesting in the past century. Radon is a radioactive noble gas; it is colorless and odorless gas and is the 86th element of the periodic table belonging to group VIII-period VI having 8 electrons in its outermost shell as well as six energy levels. Radon, initially known as radium exhalation (or niton), is one of the earliest radioactive elements, and its discovery dates back to 1900 when Fedrich Ernst Dorn, a German Physicist/Chemist, was studying the decay chain of radium. Radon has several isotopes (about 35) isotopes, most of which are short-lived and radioactive as well. Despite the littleness of their half-lives, some still live long enough to be observed in nature. Studies have reported the effects of radon and its progeny on health when being exposed for a long time via continuous inhalation or perhaps direct ingestion into the body system, this health concern it poses to humanity has attracted more attention to its study [22, 24-26].

Table 2.1 shows the decay chains of the primordial radionuclides (232Th, 235U, and 238U) known as Natural Occurring Radioactive Materials (NORM). These chains are in secular equilibrium with their daughters. The most prominent long-lived isotope of radon radionuclide is ^{222}Rn having $t_{1/2}$ = 3.82 days and its parent Radium (^{226}Ra) are generated from Uranium (^{238}U) decay series (Table 2.1-column 3). The radionuclide of shorter half-life of 55.6 sec is thoron (^{220}Rn), with its parent Radium (^{224}Ra) generated from the Thorium (^{232}Th) decay series (Table 2.1-column 1). The last radionuclide of shortest half-life of 3 to 4.0 sec is Actinon (^{219}Rn) and its parent Radium radionuclide (^{223}Ra) generated from Uranium (^{235}U) decay series (Table 2.1-column 2) [24,26].

These radioisotopes can be found in volcanic fumaroles (hot sulfurous) gasses where the gas is transported rapidly from the generation zone to the measuring point [24].

The mechanism which its isotopes are produced involves an alpha decay of the mother nuclides; there are almost 14 or more radionuclides headed by ^{238}U. Table 2.1 shows the chain starting from the head directly to the nuclei of interest, conveying the decay through possible radionuclides up to the final ^{210}Pb [20]. The Isotope ^{222}Rn will be referred to whenever the name radon is mentioned in future discussions owing to the natural abundance of its mother natural uranium (238) over the other isotope's parent nuclei.

2.2.1. Physical Properties of Radon

Radon is currently the densest known gas having a density at STP of about 9.73 $kg/m^{3,}$ which almost eight times denser than the atmosphere 1.225 kg/m^3. This is no surprise when one contemplates the fact that its decay chain alone consists of other heavy nuclides such as polonium, bismuth, and lead (see Table 2.1), and its decay is accompanied by the emitting an alpha particle (helium atom) with the energy of approximately 6 MeV. As a monoatomic gas, the element forms fcc lattice when solidified, and its physical state is retained in the gaseous form at 0 °C and 760 mm Hg (or 101.325). Other properties of radon are tabulated in Table 2.2 below [27].

Table 2.1. Uranium and Thorium decay series [20]

Nuclide	**^{232}Th decay series**			**^{235}U decay series**			**^{238}U decay series**	
	Half-life	mode of decay	Nuclide	Half-life	mode of decay	Nuclide	Half-life	mode of decay
^{232}Th	$1.4x10^{10}$y	α	^{235}U	$7.13x10^{8}$y	α	^{238}U	$4.5x10^{9}$y	α
^{228}Ra	5.75 y	β	^{231}Th	1.06 day	β	^{234}Th	24.10 day	β
^{228}Ac	6.13 h	β	^{231}Pa	$3.43×10^{4}$y	α	^{234}Pa	1.17 min	β
^{228}Th	1.913 y	α	^{227}Ac	22 y	α (1.4%) β(98.6%)	^{234}U	$2.5x10^{5}$y	α
^{224}Ra	3.66 day	α	^{227}Th	18.7 day	α	^{230}Th	$7.5x10^{4}$y	α
^{220}Rn	55.6 sec	α	^{223}Fr	21.8 min	β	^{226}Ra	1602 y	α
^{216}Po	0.16 sec	α	^{223}Ra	11.43 day	α	^{222}Rn	3.85 day	α
^{212}Pb	10.64 h	β	^{219}At	56 sec	α	^{218}Po	3.1 min	α
^{212}Bi	1.01 h	α(36%) β(64%)	^{219}Rn	3.96 sec	α	^{218}At	1.5 sec	α
^{212}Po	$3x10^{-7}$ s	A	^{215}Bi	7.6 min	β	^{214}Pb	27 min	β
^{208}Tl	3.1 min	β	^{215}Po	$1.8×10^{3}$ sec	α	^{214}Bi	19.9 min	β
^{208}Pb	(stable)	(stable)	^{215}At	$1×10^{-7}$ sec	α	^{214}Po	$1.6×10^{-4}$sec	α
			^{211}Pb	36.1 min	β	^{210}Tl	1.30 min	β
			^{211}Po	25.2 sec	α	^{210}Pb	22.6 y	β
			^{211}Bi	2.14 min	α	^{210}Bi	5.01 day	β
			^{207}Tl	4.77 min	β	^{210}Po	138.4 day	α
			^{207}Pb	(stable)	(stable)	^{206}Hg	8.2 min	β
						^{206}Tl	4.20 min	β
						^{206}Pb	(stable)	(stable)

Table 2.2. some Properties of Radon [27]

Property	**Value**
Electronic configuration	[Xe] $4f^{14}$ $5d^{10}$ $6s^{2}$ $6p^{6}$
Electrons per shell	2, 8, 18, 32, 18, 8
Atomic number (Z)	86
Melting point	202 K(−71 °C, −96 °F)
Boiling point	211.5 K (−61.7 °C, −79.1 °F)
First ionization energy	1037 KJ/mol
Molar heat capacity	5 R/2 = 20.786 J/(mol·K)
Thermal conductivity	$3.61×10^{-3}$ W/(m·K)
Phase at stp	gas
Density at stp	9.73 kg/m^{3}

2.2.2. Radon and Progeny

The fundamental origin of radon, thoron, actinon and other radon isotopes in the crust of Earth can be traced by looking at the relative abundances of radionuclides involved in the decay chain of long lived primitive radioisotopes everywhere (radium, uranium and thorium see Table 2.1). These mother nuclei, in a natural manner, buried a few meters were buried inside the crustal plate in rocks and soil, as well as in water. Uranium and Thorium are present almost everywhere in a minute or large quantities in mines, coal plants, minerals such as limestone, sedimentary rocks, granite, quartz, silicon, clay minerals, in surface/underground water and many other processed products which are extracted from minerals [26].

^{238}U decays at a rate of about 12000 atoms per second or1 mole of ^{238}U emits 3×10^6 alpha particles per second, and so do the subsequent radionuclides produced in the decay chain. In a natural uranium, the isotopes by their percentage weight are ^{238}U - 99.274%, ^{235}U - 0.720% and ^{234}U - 0.0054% [28]. It is therefore perceived that the decay series headed by ^{238}U preponderate over the actinium series ^{235}U in the environment, thorium, on the other hand, is also prevalent in some areas of the crustal plate. It is also worthy knowing the ^{238}U has a half-life ($t_{1/2}$ = 4.51 billion years) and is nearly the estimated age of the Earth. The parent nuclei of ^{222}Rn, ^{226}Ra has 1600 years half-life and in the form of chlorides or other water-soluble compounds can be found in rocks buried a few meters within the top soil or in water supplies from lakes and streams to the extent of 0.5-50 Bqm^{-3}. Water drawn from wells will generally have a higher ^{226}Ra concentration than those from surface waters. Whereas sea water was reported to contain a relatively low concentration of about 4 Bq m^{-3} [28, 29].

The isotopes polonium and bismuth are the main decay products of ^{222}Rn in the atmosphere (Table 2.1 and Figure 2.3) that can exist in their brief lifetime as ions or free atoms before attaching to solids, on moisture particles, or dust in the form of aerosols, forming molecules. ^{222}Rn decays firstly by emitting an alpha particle having energy 5.5MeV resulting in the production of ^{218}Po which within its brief lifetime decays to the first lead ^{214}Pb isotope and then the process continues where ^{214}Pb also decays to bismuth by emitting beta particle and up to the final and most stable in the entire ^{238}U series. More details on the energies and recoil distances associated with these progenies can be found in [28].

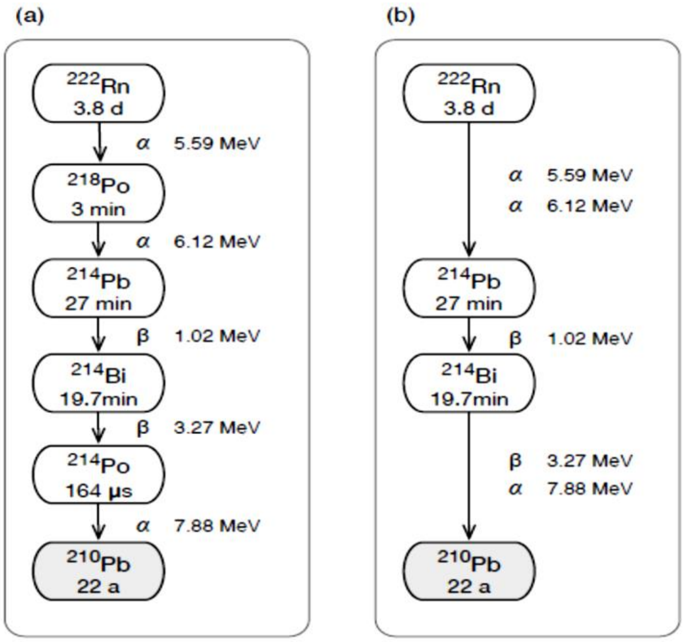

Figure 2.3. (a) Real ^{222}Ra decay series. (b) The simplified decay chain to be considered in recurrence relations [23]

Equations 2.12 to 2.15 are based on the assumption that the activity of ^{214}Po and ^{214}Bi are always the same as they are in secular equilibrium. Accordingly, the beta particle emitted by ^{214}Bi follows immediately with the alpha decay of ^{214}Po so that the ^{214}Bi decayed directly to ^{210}Pb by emitting α and β particles; this justifies disappearances of the terms involving ^{214}Po in the process. The decay chain is assumed to terminate at ^{214}Bi because of the long half-life of ^{210}Pb. Moreover, the model was built on the notion that no other external influence or perturbation acts on the decay process [2]. The average specific activity of uranium in the soil is about 25.9BqKg^{-1}, 59.2BqKg^{-1} in granite (uranium-rich rock, nearly 4.8ppm), and 11.1BqKg^{-1} in a relatively uranium poor rock basalt [24].

2.2.3. Radon Production and Recoil

It's worthy to understand the mechanism in which radon is produced and transported; this will help in understanding the natural radiation environment, radon levels in houses, mining sites as well as in earthquake prediction studies. Radium-226 via an alpha decay in solid hosts produces ^{222}Rn atoms at a rate stated in chapter 2.2.2 with each atom with a kinetic energy of about 86 keV and a potential alpha energy of 19.2Mev or 3.076×10^{-12} Joules [22]. A radon potential energy of alpha $E_{Rn\alpha}$ is the sum of alpha energies released during radon decay up to ^{210}Pb [25].

^{222}Rn has a recoil range, which depends on the fluid type in pore space and the property of the host medium, i.e. in a mineral rock, in soil, in water, or any other host material. For example,

^{222}Rn, when generated, can recoil up to 95 nm in water, 64 µm in air, 38 nm in quartz, 23.5 nm in uraninite(UO_2), and 28 nm in thorite (Th, U)SiO_4. This implies that Radon generated in-depth greater than its recoil range might not be able to escape from its host to any adjacent pore space; or in other words, the probability of ^{222}Rn escaping its host material is related to the how close to the surface its generation occurred. This will, in turn, help in understanding the mechanism in which ^{222}Rn is transported [29].

2.2.4. ^{222}Rn Emanation (ε) and Transport

Radon emanation coefficient (or emanating power) is a measure of the radon fraction in-host material generated that escapes and enters a nearby pore space or (in soil) enters into the soil pore volume; Emanation coefficient plays a role in understanding soil radon exhalation rate. The influence of some physical factors can enhance or deter radon emanation process; for example, the chemical properties and mobilization of the mother nuclide (^{226}Ra) or even the host mineral, heterogeneity in host composition and lattice structure can lead to an increase in emanation coefficient (e.g., internal porosity) whereas homogeneity slows it down. The temperature has displayed a weak effect on the emanation, while moisture plays a great role in decreasing it [25]. Soil radon is basically distributed in any of the following four states: (1) bound within the solid grains, (2) sorbed into the surface of soil grains as sorbed phase, (3) dissolved in water contained in the soil pores (aqueous phase), and (4) dispersed within the gas contained in the soil pores (gas phase). There are several ways of theoretically or experimentally estimating radon emanation coefficient (ε) depending on the parameters considered. One way of calculating ε from soil-sedimentary mineral grains in terms of the production rate of radon P (Bq m^{-3} s^{-1}), its decay constant $\lambda = 2.1\times10^{-6}$ s^{-1}, the density of dry soil ρ kg m^{-3}, and parent isotope activity concentration in solid C_{Ra} (Bqm^{-3}) is given below [30].

$$\varepsilon = \frac{P}{\lambda \rho C_{R\alpha}} \tag{2.17}$$

The value for radon emanation power varies over a wide range depending on the host material and with a typical value range of 0.2 to 30%. According to a comprehensive review by A. Sakoda et al. (2011), radon emanation for minerals, soil, and rocks are 0.03, 0.13, and 0.2 respectively. J. Porstendorfer (1994) has stated in his paper that the determination of radon flux from materials has the two steps; First, its escape from the solid mineral grains to the pores filled with air, termed "emanation ε" as described previously, Figure 2.4, and the second is a subsequent transport into the atmosphere through the pores of the material, driven by diffusion; convection/advection or other transport mechanisms [25, 31, 33].

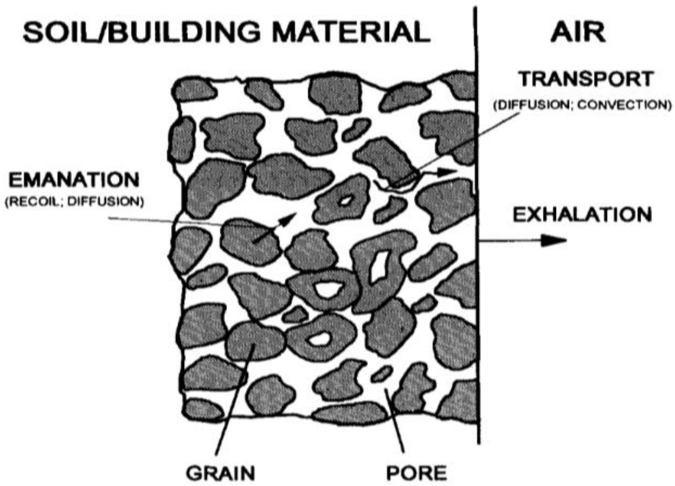

Figure 2.4. Tools of exhalation of radon and thoron from soil [29]

Figure 2.5 summarizes radon generation in soil, transport, and migration up to its entry into the atmosphere and buildings. The boxes in the figure represent the major steps using which radium in the soil gives rise to airborne radon and the horizontal arrows are labeled with names of the processes in which this transition occurs. The Labels on vertical arrows designate parameters that influence the progress rate from one state to another. The diagonal arrows denote radon loss by radioactive decay [25].

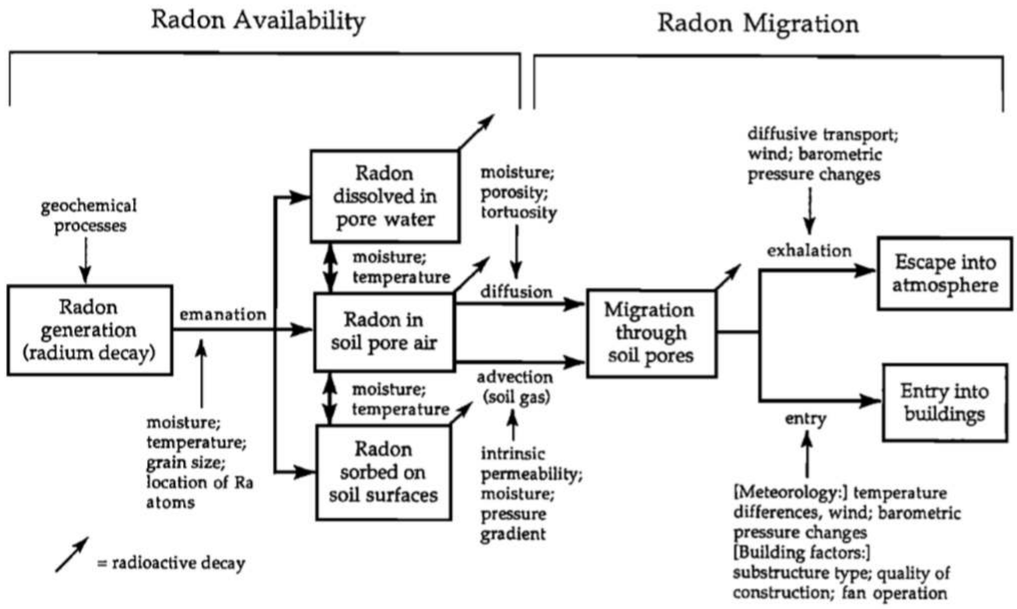

Figure 2.5. Radon generation and migration from soil to the atmosphere [25]

Radon when successfully enters into the soil pore space can be transported by two basic mechanisms;

1) Diffusive transport; using (Fick's law), for which the radon diffusive flux density J_d (Bqm^{-2}s^{-1})at a given depth in the z-direction is given by

$$J_d = -D_e \frac{\partial C_{Rn}}{\partial z} \tag{2.18}$$

or generally for 3-Dimensions

$$J_d = -D_e \nabla C_{Rn} \tag{2.19}$$

Where D_e is the radon effective diffusion coefficient (m^{2}s^{-1}), D_e in the soil of low moisture content is 3×10^{-6} m^{2}s$^{-1,}$ which is small compared to its value in open-air 1.2×10^{-5} m^{2}s^{-1} and can decrease with an increase in soil moisture content? ∇ is the gradient operator (m^{-1}) and C_{Rn} radon concentration of pore air or in water (Bqm^{-3}) with a typical indoor concentration of 50 Bqm^{-3} and for soil is between 20-10^3 Bqm^{-3} [32, 33]. The radon activity released/surface of the earth/unit time (radon exhalation rate) can be understood with J_d and has a worldwide estimation of approximately 0.015 Bqm^{-2}s^{-1} [25], but can have higher values depending on the geochemistry of the monitoring site. A simple model for soil radon transport in equilibrium condition (assuming no transport mechanism other than diffusion) can in words be written as;

Radon accumulation = Production (q) - Decay + Diffusive transport

Mathematically;

$$\frac{\partial C_{Rn}}{\partial t} = q - \lambda_{Rn} C_{Rn} + D_e \nabla^2 C_{Rn} \tag{2.20}$$

Or when taking into account many other factors in the flow, we have

$$(\varepsilon_a + \kappa\varepsilon_W + \rho K)\frac{\partial C_{Rn}}{\partial t} = \rho\varepsilon A_{Ra}\lambda_{Rn} - (\varepsilon_a + \kappa\varepsilon_W + \rho K)\lambda_{Rn} C_{Rn} + \varepsilon_a D_e \nabla^2 C_{Rn} \tag{2.21}$$

Where; $\varepsilon_a,\ \kappa,\ \varepsilon_W,\ K,\ \rho,\ \varepsilon\ and\ A_{Ra}$ are respectively the air-filled soil porosity coefficient, dimensionless partition coefficient (connecting radon equilibrium specific activity in air to that in water and is a function of temperature), water-filled soil porosity coefficient, partition coefficient for sorption (m^{3}kg^{-1}), dry bulk density of soil (kgm^{-3}), emanation coefficient of earth or rock and the radium content of soil (Bqkg^{-1}). And all other terms have their usual meanings. As described by Henry's law, The partitioning of gas with aqueous phases as well as that between gas and sorbed phases are respectively given as [25, 31]:

$$C_{Rnw} = \kappa C_{Rn} \qquad and \qquad C_{Rns} = K C_{Rn} \tag{2.22}$$

Where C_{Rnw} is the concentration of radon in water (Bqm^{-3}) and C_{Rns} represent the sorbed radon concentration in dry soil (Bqkg^{-1})

2) Advective transport (Darcy's law); relates the flow rate per unit cross-sectional area (the superficial velocity vector v_d) to the the dynamic or disturbance pressure gradient ∇P given as:-

$$v_d = \frac{k_p}{\mu_a}\nabla P \quad (2.23)$$

Where, k_p and μ_a are respectively the intrinsic permeability of soil (m^2) and dynamic viscosity of air (kgm^{-1}s^{-1}). And therefore, radon activity flux per unit pore area due to advection is given by [25], [34]:

$$J_a = v_d C_{Rn} \quad (2.24)$$

or in soil air with air-filled porosity ε_a we have

$$J_a = \frac{v_d}{\varepsilon_a} C_{Rn} \quad (2.25)$$

The total radon flux J_{da} from the soil accounting for both advection and diffusion flow is then obtained by summing up, Equations 2.19 and 2.24 as follows;

$$J_{da} = v_d C_{Rn} - D_e \nabla C_{Rn} \quad (2.26)$$

And general transport equation for radon in the air-filled pores that account for both advection and diffusion under the following assumptions is given in Equation 2.24 as stated by Nazaroff (1992):

(1) Linear equilibrium relationships describe phase partitioning among gaseous, aqueous, and sorbed states.
(2) The transport process occurs only in the gas phase.
(3) Diffusive and advective transports are described by Fick's and Darcy's laws.
(4) Air is treated as an incompressible fluid.
(5) Permeability, porosity, and diffusivity are constant in space and over time and
(6) Mechanical dispersion is negligible.

If this assumption is not valid, then the coefficient D_e must be replaced by a mechanical dispersion coefficient, which is a function of the fluid velocity through the soil.

$$(\varepsilon_a + \kappa\varepsilon_W + \rho K)\frac{\partial C_{Rn}}{\partial t} = \rho\varepsilon A_{Ra}\lambda_{Rn} - (\varepsilon_a + \kappa\varepsilon_W + \rho K)\lambda_{Rn}C_{Rn} + \varepsilon_a D_e \nabla^2 C_{Rn} + \frac{k_p}{\mu_a}\nabla C_{Rn}.\nabla P \quad (2.27)$$

Most researchers prefer to use a simplified version of Equation 2.27 in their study, often define radon accumulation in terms of the total flux density, production (q) and loss with all symbols maintaining their previous definitions;

$$\frac{\partial C_{Rn}}{\partial t} = q - \lambda_{Rn}C_{Rn} - \nabla.J_{da} \quad (2.28)$$

$$\frac{\partial C_{Rn}}{\partial t} = q - \lambda_{Rn} C_{Rn} + D_e \nabla^2 C_{Rn} - \nabla.(\nu_d C_{Rn}) \quad (2.29)$$

The production rate q is sometimes defined differently $q = \rho \varepsilon A_{Ra} \lambda_{Rn}$, depending on the study.

2.2.5. Radon in atmosphere

Despite the fact that many researchers neglected or ignored the effect of natural radioactivity on the atmospheric morphology (the Earth's gaseous invasive crust). It plays an large part in atmospheric morphology. Radioactive emission of the radionuclides can be represented by electromagnetic radiation (γ and X-rays) or particles (β, α, protons, neutrons).

Radiation ionizes and excites surrounding atoms and molecules. The main sources of ionization in the lower atmosphere are Earth's natural radioactivity and air, as well as human sources and cosmic rays. Many sources of hazardous radiation contribute in exposing people to the significance health risks, as reported in NCRP (report No. 93) and shown in the pie chart Figure 2.6. Ionization of natural radiations of ground represent about 60% compared to the general productivity of natural sources, such as in soils. However, as the chart shows, radon is the source of more than half (55%) of a typical individual's radiation dosage from common causes. The main radionuclide radon and its progenies are a primary source of the α-particles (of a charge +2e) with energy limits of 4 – 9 MeV [35].

It is obvious that after radon emanation process and soil exhalation exist, radon passes to the near ground air levels and diffuse to the atmosphere. A constant diffusion exists horizontally at near ground levels, while the vertical diffusion of the radionuclides tends to move up rapidly while their concentrations die out exponentially due to decay.

As reported in literatures that the atmosphere contains 78% nitrogen and 21% oxygen by volume, while the remaining 1% trace gases as well as water vapors moving freely in air. As the concentration of aerosol particle is higher during the day and lower at night, radon progenies (^{218}Po, ^{214}Pb, ^{214}Bi, and ^{214}Po) Quick attached to aerosol particles, attracting associated atmospheric ions [23].

Vertical distribution of radon and its progeny in atmosphere up to a height of 12 km is influenced by turbulent air mixing, eddy diffusivity, decay constant of these radionuclides as well as the dry and wet removal of atmospheric aerosols [23].

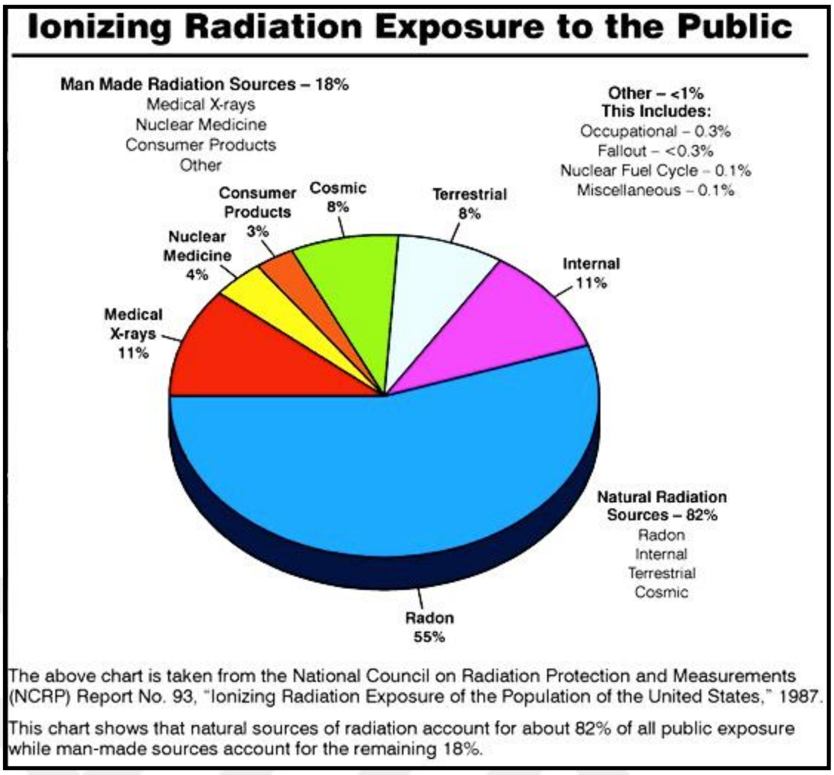

Figure 2.6. Ionizing radiation exposure to the public [35]

2.2.6. Uses and Health Effects

Radon gas plays a role in variety of applications, some of which include atmospheric tracer in atmospheric transport processes, selection of marine air masses least-perturbed for baseline studies, terrestrial air mass movements tracing, including refinement of source footage for aerosols in continental outflow events, calibration of regionally integrated greenhouse gas emissions, electric field studies and the lower atmosphere of vertical mixing quantification. The survey of radon in soil, water, and the atmosphere is essential when it comes to understanding radioactivity in the atmosphere [36].

On the other hand, radon poses a health problem to humans. Radon can only be of harm when ingested or inhaled (in the form attached to aerosols) into the body and continues to irradiate the inner tissues with alpha particles, competing with all the deposition, absorption, clearance, and translocation processes that take place in the human system as it has been carried along [22].

Owing to that radon accounts for most of the terrestrial radiation exposed by humans, two-thirds of radiation dose received by living tissue is believed to have been caused by radon and its progeny. Cancer lung is currently the main health concern, which is associated with radon exposure. Cancer is mostly thought to require at least one mutation to occur and then to continue to spread intermediate cells that have sustained some degree of DNA damage. This phenomenon will enormously increase the grouping of available cells for cancer growth. Even a single alpha particle can cause a cell to suffer significant genetic damage. It is then likely that damage to radon based DNA will occur at any exposure level [25, 37].

Indoor and outdoor air it is ubiquitous and many underground mines are contaminated. Enormous epidemiological evidence from miner studies and comparable data on animals has reported that radon in smokers and even non-smokers causes' lung cancer. Radon have to be treated as a potentially important cause of cancer of lung for the general public, which is subjected to radiation and contamination by radon indoor air from soil, water, and other construction materials.

Alpha particles are large and fairly highly charged, but not penetrative, and are easily blocked by clothing or epidermal tissue provided the source remains outside the body. However, when absorbed, alpha particles can cause tissue damage, and since they are not penetrative they give up their energy to a comparatively limited tissue volume. The main pathway through which alpha activity enters the human body is through inhalation of radon and, more pertinently, its direct daughter products, which are also emitters of alpha particles. Since radon is a noble gas, and its half-life is 3.82 days, most radon is again breathed out. However, the daughter products, which remain as suspended aerosols, can remain in the respiratory system on dust and moisture particles or are unattached, becoming solid.

An effect on humans; radon as an atom is not hazardous and it is chemically inert gas. It doesn't accumulate in the body to any great extent. Rather, the main concern is the short-lived degradation of radon products (i.e., the isotopes represented by shaded boxes in Figure 2.4. These contaminants are chemical reactive and can thus be stored in the tissues of the respiratory tract when inhaled [29].

Radon levels are used directly to control indoor (dwellings and also most places of work) or outdoor levels of radon. However, the calculation of the effective dose is crucial, which can be derived from the equivalent dose. Equivalent dose (H_T) in millisieverts (mSv) is calculated for individual organs and based on the absorbed dose (D) to an organ for a given dose accumulation period time (conventionally 50 years of exposure). The equivalent dose is adjusted to account for the effectiveness of the type of radiation (tissue weighting factor Q_T) such that.

$$H_T = D \times time \times Q_T \tag{2.30}$$

Effective dose (E_T) in mSv is calculated for the whole body. It is a summation of equivalent doses of all organs such as:

$$E_T = \sum_T H_T \tag{2.31}$$

ICRP has developed and simplified the calculation of the equivalent dose and the effective dose for inhaled or ingested radionuclides [22].

Breathing air with 50 Bq / m^3 of radon (a standard global value in buildings) for one year at work (2000 hours) provides an effective dose of 0.7 mSv, using the dose ratio for most occupational exposure circumstances. The prescribed dose coefficient is higher for work indoors performing heavy physical exercise or for exposures in tourist caves, so breathing air with 50 Bq/m^3 of radon at work for one year provides an effective dose of 1.4 mSv [38].

2.2.7. Radon Detection

Radon and its progeny in a clear atmosphere can be detected to an elevation as high as 3500 m [23].

The detectors used in monitoring radon activity are divided into two categories; the first category is a family of “active detectors” and is capable of giving real-time events of radon in a given area. While the second category is that of the “passive detectors,” which needed to be taken to the laboratory for further detection procedures after being exposed to radon radiation dose for a given time. The solid-state nuclear track detectors CR-39 (semi-conductor based) is the most common amongst the types of passive radon detectors [39]. While the radon spectroscopy RAD7 (DURRIDGE Company Inc.) is a well-known example of an active detector. Other common detectors are ZnS (Zinc sulfide) scintillator and the Barasol (Algade, France) probe, which detects and measures radon gas via diffusion. Radiation detectors are primarily designed to be capable of producing ionization when hit by of radioactive particle or perhaps generate a signal (e.g., electric signal), which is, in turn, used to estimate the magnitude of the detected activity. An example of using ZnS (Ag) is the determination of the gross alpha concentration of four locations in Sivrice Fault Zone of the East Anatolia Fault System. It is seismically active and often produces earthquakes of varying magnitudes (just about 2.0-4.5 Md). The concentration of radon in the found fault zone is substantially higher than that of other regions [29].

Other examples of radon detection devices can be found in the literature [40]. Radon also can be detected indirectly by using the activity of its progenies. For example, ^{214}Pb produces a peak of gamma at 351.9 keV in fluids when analyzed using high-purity germanium (HPGe) detector [29, 41].

3. MATERIALS AND METHODS

MATLAB code is used to perform statistical analysis of time series and atmospheric electric field. ARIMA and Monte Carlo models that build in MATLAB are adopted for such purpose. Atmospheric Total Electron Content, its variability Near-Ground atmospheric layers and radon and seismic signatures in the ionosphere will be discussed. Finally to provide a brief overview to the topography, geology, and climate of Anatolia and Erzincan basin as study area.

3.1. Time Series Statistical Analysis

Time series is a continuous sequence of data observation points $x(t)$, usually calculated over successive time periods t = 1,2,3,..., of discrete and equally spaced intervals like minutes, hours, days, weeks, months or years separations, where x(t) is a random time dependent variable [42].

3.1.1. Time Series Behaviors

In general the time series might be characterized and affected by one or more of the following four components:

Trend, is a long term movement in a time series. I.e. an inclination of a time series toward increasing, decreasing or become stagnant over a long time period.

Cyclical, is a periodic time series that repeat itself in cycles over longer period.

Seasonal, is a seasonal fluctuations of a time series within a year. Climate and weather conditions, customs and habits are the main factors affecting seasonal variations.

Irregular, is a random variation in a time series. Irregularity happened by unpredictable events caused incidentally by war, strike, earthquake or flood, etc.

The stochastic process of a time series $(x(t), t = o, 1, 2, ...)$ is to be stationary of any order k as a statistical equilibrium if the probability distribution function (s) connecting values of $x_{t-s}, x_{t-s+1}, \dots, x_t, \dots, x_{t+s-1}, x_{t+s}$ depend only on time differences and is independent on time (t) for any value of s. It is a needful condition to build a model that is used for future prediction. Statistically, mean and variance of a stationarity process is time independent so one can reduce the complexity of the fitted model [43].

Practically, it is normal that time series having Trend or Seasonal patterns are naturally non-stationarity. Time series that show non-stationarity are those contain trend and seasonal patterns, among them radon concentration in seismic region, stock price, socio-economic and business [43].

3.2. Time Series Modeling

A dynamic modeling is used to analyze time series data. Recently, researchers pay attentions to develop various models. The goal of such statistical modeling is to collect data or previous observations of a time series as a basis and then build a suitable model explaining the series' principal actions. The most important goal is to forecast and predict the future values of the chain from the understanding of the past. Because of the vital valuable of forecasting of time series, a fitting of a proper model is used in various practical fields, mainly in science, engineering, business and economics [42].

MATLAB is a software package consists of multiple functions used for modeling and analyzing different time series data. It has a capability to provide a wide range of diagnostic tests, such as impulse analysis, unit roots and stationarity, and structural change [74].

For the purpose of statistical analysis, different time series forecasting models have been developed. Among many stochastic models frequently used are the Auto-Regressive Integrated Moving Average (ARIMA) and Monte-Carlo simulations to forecast time series observations that build in MATLAB software package. In addition, EXCEL software is helpful.

3.2.1. ARIMA(*p;d;q*)

ARIMA (p; d; q) models were developed to include the status of non-stationary time series data. It is a generalization of the ARMA model, which applies only to stationary time series.

Assuming the linearity of the time series and following the normal distribution is the basic assumption to implement this model. The three subclass models controlling the stochastic ARIMA model are: the Autoregressive (AR) that manipulate the dependency of an observation with some rest lagged observations, and Moving Average (MA) that manipulate the dependency of an observation with residual error applied to lagged observations, both sub models adopted from (ARMA) model and work on stationary time series. Adding Integrated (I) to make the time series stationaries by using the differencing of raw observations. These sub models in ARIMA considered as controlling parameters [44] [43].

A standard notation of the model is ARIMA(*p;d;q*) where the three variables (***p;d;q***) are defined as follows:

p for AR(*p*) model, is the lag order representing number of lag observations.

d for I, is the degree of differencing defining as the number of times that the raw observations are differenced.

q for MA(*q*) model, is the order of moving average giving size of the moving average window.

The three above parameters are given by integer values to identify the specific ARIMA model.

The mathematical expression of AR(p) series model of the order p A linear combination of past observations (p) and a random error called a random shock can be represented (ε_t). Then the governing equation to compute the future value of a variable (y_t) at time t is given as [43]:

$$y_t = c + \varphi_1 y_{t-1} + \varphi_2 y_{t-2} + \cdots + \varphi_P y_{t-P} + \varepsilon_t = c + \sum_{i=1}^{p} \varphi_i y_{t-i} + \varepsilon_t \qquad (3.1)$$

where c is a constant, it might be omitted sometimes just for simplicity and φ_i ($i = 1, 2, 3, \ldots, p$) are model parameters.

Similarly the mathematical expression of MA(q) series model of an order q can be represented by using the past random shock (ε_t) as explanatory variables. Then the governing equation to compute the future value of a variable (y_t) is given as [43]:

$$y_t = \mu + \theta_1 \varepsilon_{t-1} + \theta_2 \varepsilon_{t-2} + \cdots + \theta_q \varepsilon_{t-q} + \varepsilon_t = \mu + \sum_{j=1}^{q} \theta_j \varepsilon_{t-j} + \varepsilon_t \qquad (3.2)$$

where μ is the series mean and θ_j ($j = 1, 2, 3, \ldots q$) represent model parameters.

The white noise process derived from random shocks is an ordered of separated random variables distributed identically as (i.i.d) with a mean (μ = 0) and a constant variance σ^2.

Combining the two polynomial Equations 2.31 and 2.32 together come out by a general and useful of ARMA model to find the future value of a variable (y_t).

$$y_t = c + \varepsilon_t + \sum_{i=1}^{p} \varphi_i y_{t-i} + \sum_{j=1}^{q} \theta_j \varepsilon_{t-j} \qquad (3.3)$$

In term of the lag operator notation L, Equation 2.34 can be written as $Ly_t = y_{t-1}$. Now the two Equations 2.31 and 2.32 are; $\varepsilon_t = \varphi(L)y_t$ and $y_t = \theta(L)\varepsilon_t$ respectively. Here:

$$\varphi(L) = 1 - \sum_{i=1}^{p} \varphi_i L^i \ \ and \ \theta(L) = 1 + \sum_{j=1}^{q} \theta_j L^j \qquad (3.4)$$

A non-stationarity time series can be stationaries by inserting an integer d, which controls the level of finite differencing in ARIMA(p,d,q) model. Then in terms of lag polynomials the expression can be written as:

$$\varphi(L)(1-L)^d y_t = \theta(L)\varepsilon_t \qquad then$$
$$\{1 - \sum_{i=1}^{p} \varphi_i L^i\}(1-L)^d \, y_t = \{1 + \sum_{j=1}^{q} \theta_j L^j\}\varepsilon_t \qquad (3.5)$$

As mentioned before, the values of p, d, and q are integer and equal and greater than zero, i.e. 0, 1, 2, 3… These values indicate the order of each sub-model (autoregressive AR(p), integrated I(d) and moving average MA(q)), for instant 0 value of any one means omitting that sub-model. It is worthwhile to mention that choosing d = 1 is adequate in almost all cases.

3.2.2. Stationarity Evaluation

After the above brief review of ARIMA(p,d,q) time series model, it is obliged to know how to select optimal orders of the model which reduces the non-stationary time series to be stationary so that creating accurate forecast depending on a description of historical pattern of the data.

For do so, the Autocorrelation function ACF and the Partial Autocorrelation function PACF need to be evaluated. In addition to that was proved by Box and Jenkins [46], Hipel and McLeod reported another simple method to determine the stationarity of an AR(p). For instance,, the AR(1) model $y_t = c + \varphi_1 y_{t-1} + \varepsilon_t$ is stationarity if $|\varphi_1| < 1$, with mean μ constant and variance γ_0 of [43]:

$$\mu = \frac{c}{1-\varphi_1} \qquad and \qquad \gamma_0 = \frac{\sigma^2}{1-\varphi_1^2} \tag{3.6}$$

Other commonly used methods are the Akaike Information Criterion (AIC) and the Bayesian Information Criterion (BIC), described in the [45].

3.3. Monte-Carlo simulations

Monte Carlo methods refer to a class of methods to solve mathematical problems using random samples. Generally speaking, Monte Carlo methods used for solving deterministic problems and the computation of the expectation value of a random variable. The fundamental idea behind using the Monte Carlo method is to run simulations over and over to get a distribution of probability of an unknown stochastic entity. In many cases, numerical methods such as Monte Carlo are helpful when analytical methods are too difficult to solve or fail. Monte Carlo methods represent number of groups of computational algorithms and techniques for simulation solution that rely on repeated random selection. The underlying idea is to use random nature to solve issues that, in theory, might be probabilistic [46].

Scientists working on the atom bomb first used the technique; the name was adopted from the resort town of Monaco famous for its casinos. Monte Carlo simulation has been used since its invention in World War II to model a range of physical and analytical structures. Monte Carlo simulation is a methodology used to understand the effect of risk and uncertainty in various fields of science, engineering, finance, project management, cost, and other forecasting model. A simulator in Monte Carlo helps to visualize most or all of the potential outcomes to get a better idea about the risk of a decision [47].

Working on Monte Carlo simulation in MATLAB code begins by random generation of "N" inputs or scenarios, and then runs a simulation for each of the "N" inputs. Simulations are performed on a computerized model of the analyzed method. Then summarize and evaluate the outputs from the simulations. Many built in functions in MATLAB; all generate time series level forecasts to simplify the study of accuracy and the comparison of forecasts from the alternative models. Taking arguments about time-series levels as inputs and perform the appropriate transformations. It calculates outcomes over and over again, using different set of random values from the probability functions. Simulation of Monte Carlo could involve thousands or tens up to thousands of pairwise comparisons before complete [48].

The present problem definition of radon concentration time series is that the radon observations are irregular, random, unpredictable data in its variation with time and strongly affected by earthquakes, also to some extent affected by meteorological conditions of the region. So the studied system is modeled in MATLAB code by a set of random input variables, which will be collected into a vector, (Y) as a probability distribution then set of output variables or scenarios will be assembled into a vector, (X). As these outputs are depending on the random inputs, they must be random variables as well. However, since the probability distribution of the outputs is not known, the objective of simulating is to determine the behavior of the outputs or in other wards set of forecasting distributions.

3.4. Atmospheric Total Electron Content

The ionosphere in the upper atmosphere is regarded as a conducting layer. In understanding the precursory of earthquakes, a relationship between electric field and the total electron content (TEC) of atmosphere with radioactivity plays an important factor.

3.4.1. Atmospheric Plasma

The matter is classically graded as 'solid, liquid, and gas' in three states. It modifies its original states by adding more and more energy to matter: from solid to liquid, then from liquid to gas. Also adding more energy to the gas results in ionization processes in which gas atoms and molecules are separated into excited, reactive charged particles such as ions, radicals and free electrons as shown in Figure 3.1. This energy supplied can be either thermal or transmitted by electrical or electromagnetic radiation. This medium, called plasma, is chemically active and is considered 'the fourth state of matter' and constitutes more than 99 percent of the universe. Plasma state is ended by removing the external energy, and then by combing of the free electrons with positive atoms the medium returns to the gas state [49].

The generation of plasma of low or very high 'temperatures' depend on the way of activation and their working power which can be referred as cold and thermal plasmas. The plasma is considered 'hot' when all the particles are in thermodynamic equilibrium (have the same energy), while if the electrons have higher energy than the ions, the plasma is 'cold.' This particular condition appears under specific conditions such as low pressure or HF voltages and allows for chemical reactions at low temperatures [50].

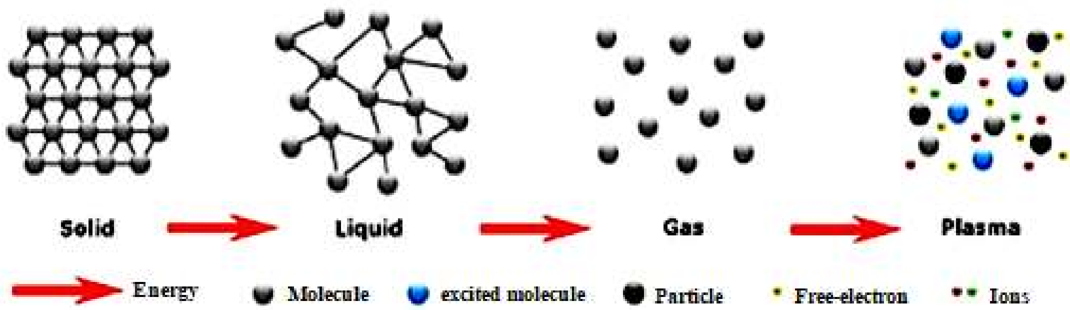

Figure 3.1. The four states of matter [49]

3.4.2. Atmospheric Electric Field

A relationship between electric field of atmosphere with radioactivity is very important specifically in understanding and precursory of earthquakes. The atmospheric electric field is also related to some other Earth's natural phenomena such as climate change [50].

The ionosphere in the upper atmosphere as regarded a conducting layer undergoes a consequence of the continuous ionization air mainly by ultraviolet radiation influenced from solar activity. The upper atmosphere has conductivity of ocean water, while lower than that of the earth crust soil. Accordingly, the ionosphere and earth's surface have qualities or features of a capacitor with air acting as an insulator having a resistance and conduction current density between them. This conceptual model is known as the global electric circuit (GEC) [51]. The atmospheric conductivity and the atmospheric electric field are shown in Figure 3.2 (a) and (b) respectively. As the ground serving as a negative electrode of this big capacitor, the potential between the ionosphere and the ground varies from 260 to 280 KeV and with field orientation downwards. Consequently, this electric field drives down positive ions, and up negative ones. The ion flux produced makes up the fair weather current. The capacitance of this circuit C_c and a columnar resistance R_c between the ground and ionosphere are of the order of $1\mu F$ and 200Ω respectively [50].

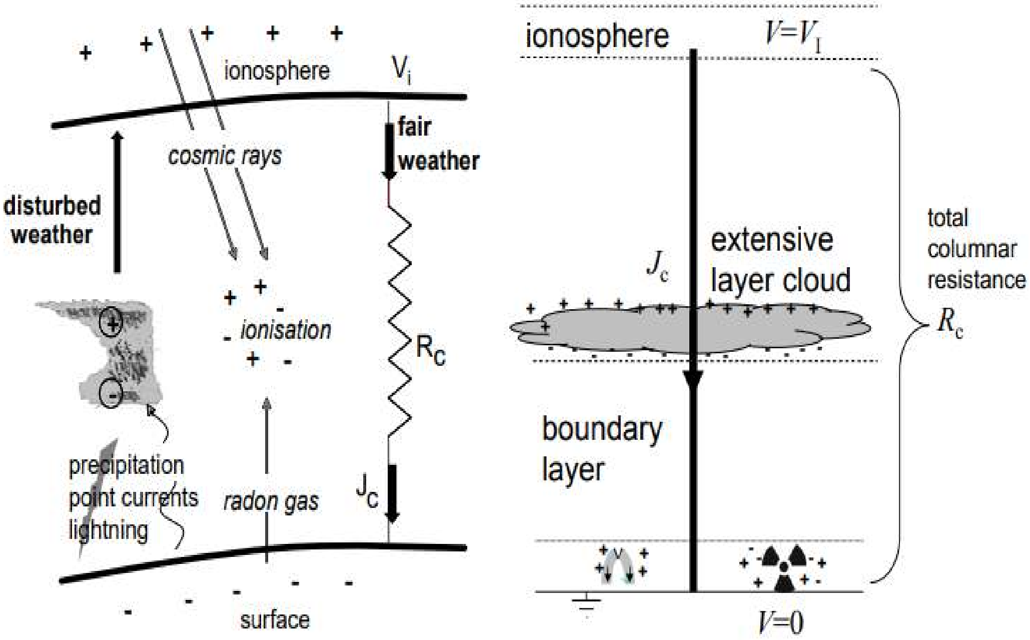

(a) **(b)**

Figure 3.2. (a) and (b), conceptual representations of the global electric circuit, [51, 52]

It is well verified that the climatic and weather conditions of the earth surface and atmosphere are changeable due to various natural parameters and factors. The atmospheric electric field consequently varies in response to climatic changes, weather conditions or other factors like smoke, pollution, meteorological parameters, seismicity, radioactivity, aerosol density, vegetation, etc. [50]. The surface atmospheric electricity in different weather conditions has been modeled and given in a standard curve known as the Carnegie curve. This curve shows the maximum and minimum values around 19:00 UT and 03:00 UT as shown in Figure 3.3. While in fair weather days, the global atmospheric electric field according to this curve can vary within the range 100– 300V/m [53]. Figure 3.3's right hand curve represents the Carnegie curve that describes daily surface Potential Gradient (PG) variations. This curve averaged from cruise measurement data (grey shading shows 95% confidence range on mean values) while the left curve is the diurnal variation of the atmospheric electric field (top panel). The negative values here mirror the direction of the electric field down [50, 53].

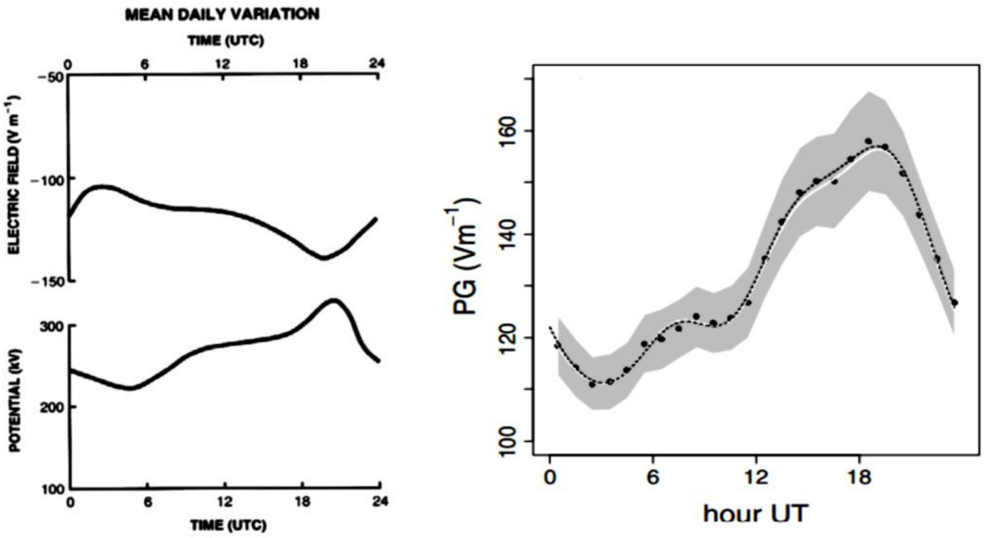

Figure 3.3. Left, the daily variation of electric potential, and Right, Carnegie curve [53]

3.4.3. The Ionosphere and Total Electron Content

The upper portion of the atmosphere is called ionosphere, where there are enough electrons and ions to interact with electromagnetic waves. The earth's ionospheric layers are classified to D, E, F1, F2 and to some extent, the C layer, depending on the type of processes that occur in each as well as the average electron density available [54].

The Total Electron Content (TEC) could be defined as the number of free electrons along one-meter-square cross section radius that extends through the ionosphere all the way up from the ground. The presence of the TEC is coming from the outer earth's environment from the interaction of the solar radiation with the chemical composition in the atmosphere. The spectrum of radiation varied from radio frequency through Infrared Radiation (IR) and X-ray. The atmosphere's strong ionized X-ray and UV region is plasma containing the charged particles; electrons, and ions. Free electrons are formed by the ionizing action of sun radiation on the upper atmosphere of the earth. The number of such free electrons above about 60 km is adequate to affect the propagation of electromagnetic waves [55].

TEC or the density of the electron columnar number is an important descriptive amount for the Earth's ionosphere. The received radio signal is proportional to the number of electrons within the radio wave direction. TEC is the best parameter to monitor possible space-weather impacts for ground to satellite communication and satellite navigation. It's measured in free electrons per square meter along the ray path, such that 1 TEC Unit (TECU) = 10^{16} electrons/m². The Earth's ionosphere TEC ranged from a few to several hundred TECU [56, 57]. Figure 3.4 shows the behavior ionospheric layers for a summer day in mid-latitudes in the day, and at night, the C-layer extends from 50-65km, the D-layer from 50-90km or 70-90km depending on the atmospheric conditions. The E-layer on average extends approximately from a height 90 to140km from within which the sporadic E-layer at the height of 115km is formed. The F-layer, in general, extends from 140 up to around 350km, consisting of the F1-layer (140-200km) as well as the F2-layer (200-350km). Above the F2-layer, the boundaries from the top extend up to one or two kilometers. F-layer contains the highest electron density making it the most crucial ionospheric layer in the context of telecommunication and other applications; Figure 3.4 displays the composition of the ionosphere in middle latitude and ionizing regions on a summer day and night [54].

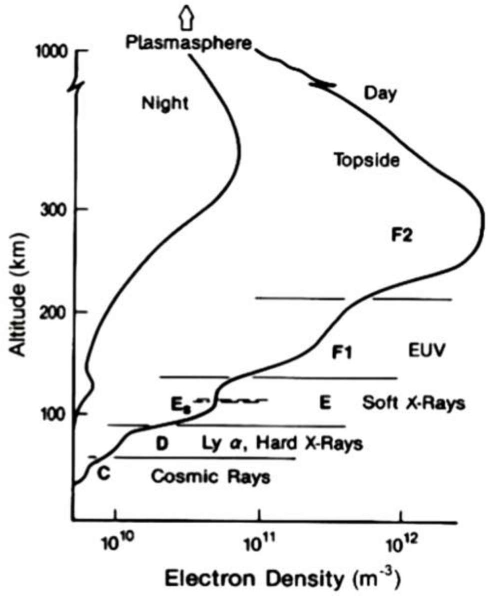

Figure 3.4. Ionosphere and its layers [28]

Earth's ionosphere layer constitutes different chemical compositions. Depending on the altitude and temperature of sub ionosphere layers the composition is varied. For instant the main composition of the lower layer D region is N_2, O_2, Ar, CO_2, He, O_3 and H_2O are present, [58, 20-22]. In addition, dust particles sustaining in the atmosphere along with some traces of Iron and Sodium received from the meteor debris. In the E and F region mainly the molecular ions like NO^+, O^{2+}, O^+ and N^{2+} are dominating. In the upper F region ions like O^+, H^+ and He^+ are present [54]. The ionosphere's TEC is changed by adjusting the Extreme Ultra-Violet solar radiation, geomagnetic disturbances, and the seismic waves that spread from the lower layer. Thus, the TEC will depend on local time, latitude, longitude, season, geomagnetic conditions, solar cycle and activity, and conditions in the troposphere. The ionosphere controls the propagation of electromagnetic waves. When the signal passes through the electrons in the ionosphere the speed of radio waves accordingly changes. The total delay suffered by a radio wave that propagates through the ionosphere depends on both the radio wave frequency and the TEC between the transmitter and the receiver. The radio waves cross the ionosphere at certain wavelengths. In other wavelengths the ionosphere reflects the waves. However, forecasting specific time scales of earthquakes from a few years to a few days is a highly complex issue. Recent studies have suggested that satellites and ground-based installations in the ionosphere may detect earthquake precursors a few hours or days before the main earthquake (Pulinets, and Liu et al.). Earthquake prediction monitoring and analysis employ a regular inspection ionosphere TEC differentiated from the GPS receiver global positioning system [59].

3.4.4. Radon and Atmospheric Electric Field

Radon and progeny in the atmosphere can be in any of the three different forms: positive small ions; positive and negative abundant ions; and neutral atoms and uncharged aerosols. It is known from the literature that the atmosphere contains 78% nitrogen and 21% oxygen by volume. Radon progeny when produced (predominantly 88% positive ions) are highly reactive (less than 1sec); They react with the remaining 1% trace gases as well as water vapors forming positive clusters of radionuclide particles moving freely in air (called unattached) and are highly mobile with diameters ranging from 0.5 to 5 nm. The mobility of these clusters is influenced by metrological conditions [29].

Radon and its progeny in a clear atmosphere can be detected to an elevation as high as 3500 m. The distribution of radon and its progeny in atmosphere up to a height of 12 km (tropopause) is influenced by turbulent air mixing, eddy diffusivity, decay constant of these radionuclides as well as wet and dry removal of atmospheric aerosols. Jacobi and Andre modeled radon and thoron concentration in a horizontally isotropic atmosphere (no horizontal gradient) and obtained plausible results when compared to experimental findings for the profile distribution of the diffusion coefficient with altitude as well as the variation of radon and its progeny concentration [60].

Wet or dry air removal methods do not affect radon concentrations, because it is an inert and rarely soluble in water. ^{222}Rn's 3.82-day half-life is equivalent to the time of residence of main atmospheric contaminants as well as the synoptic time scale. This half-life also is broad enough relative to standard turbulent time scales (~1 h); therefore, it is considered to be well adapted for tracing of air transport in the atmospheric boundary layer (ABL) and over ground studies. While, its half-life is short enough to restrict concentrations of radon in the free troposphere to usually be two orders of magnitude lower than normal ABL values. The effect is broad differences in concentration across the lower troposphere primarily related to vertical mixing processes. It is worth noting that the gap in radon emissions over land and over open water sources is around two to three orders greater in magnitude [56].

3.4.5. Variability Near-Ground Atmospheric Layers

The earth's ionosphere layers are classified to C, D, E, F1, F2 that extend from 50-65km, 70-90 km, 90-140 km, 140-200 km and 200-350 km respectively above the earth surface as mentioned in 5.2 while the lowest atmospheric layer (called near ground) may be the most important. The first shock and effect of any underground events such as earthquake is experienced by the lowest part of the boundary layer reached 50 m above ground.

Near ground atmospheric layers behave with broad vertical temperature, wind speed and humidity gradients. Atmospheric electric field or electricity near ground atmospheric layers depends on many factors or sources. Among these causes are the instability in the planetary boundary layer, cloudiness, air pollution, aerosols of various origins, such as volcanic eruptions, and natural radon and daughter products degassing from the crust of the earth. Radioactive emissions from nuclear testing and accidents like Three-Mile Island, Chernobyl nuclear reactor in April 1986, or Fukushima in 2011 accidents that released a high radioactivity to the atmosphere, consisted of a variety of radionuclides including ^{131}I, ^{137}Cs, ^{134}Cs, storms of snow and dust, typhoons, orographic impacts, etc. Some similar cases have been reviewed in Israel, Holland, and others [61, 62]. Attempts to quantify the effects of these atmospheric electric field disturbances on fluctuations in the ionosphere were made by [63].

Among the results, the emanation of radon from the crust significantly shifts the conditions of the near ground layer. This emanation will change the value of the electric field inside the layer up to the reverse sign of the effect of the electrode by several times. The potency of ionization of the radon and its progenies may be up to 10 times greater than that of cosmic rays which can influence the activity of the thunderstorm; furthermore, the surface roughness also affects the volatility of the electrical field near ground [64].

Pollution of atmospheric aerosols is another very important effect. Some experimental measurements show that the atmospheric electrical field contaminated by aerosols is up to four times higher in rural areas than in clear air, i.e. around 400 V / m versus 100 V / m. The decrease of atmosphere conductivity is the major effects of aerosols. These effects were observed in the northern hemisphere as a result of increased volcanic activity, measurements taken between 1907 and 1972 [59].

Some critical factors influence the local energy balance are the scale of the aerosol particles, and their mobility. The mobility k can be defined as the average velocity (v) that the charged particle acquires under external electric field (E) action [64]:

$$k = \frac{v}{E}\ [m^2 V^{-1} s^{-1}] \tag{3.7}$$

The small ion mobility is three orders of magnitude greater than that of large ions. This means that if the small ions are replaced by the large ions under certain conditions (as happens during the hydration process), the conductivity will drop to practically zero, which will increase the electric field sharply.

3.4.6. Radon and Seismicity (Seismic Signatures in the Ionosphere)

The discussion in earthquake prediction about the physical mechanisms of the atmospheric electric field is based on experimental evidence. The results of many recent studies can be seen as the basis for future applications, in particular the prediction of short-term earthquake. Earthquake prediction starts by coupling the ground and satellite based observations of complex systems of space borne and electromagnetic and ionosphere precursors of earthquakes, and those still under construction. While several theories for seismic-ionosphere coupling have been suggested, several points remain unanswered, in particular for the equatorial and low latitude ionosphere due to its highly dynamic conduct [57].

The exhalation of underground gases/fluids (e.g., radon) is a consequence of the continuous movement of the crustal plates, which enhances gas/fluid migration to the atmosphere via stress/strain, pressure driven flow. This is one of the reasons why radon concentration turns higher near fault lines, trenches (or a similar) than in other places. Increase or decrease in radon concentration in soil/water has been reported to have a relationship with seismicity of a given area.

The main factors causing the near ground atmospheric ionization are radioactivity and cosmic radiation as shown in Figure 3.2. The variability in surface and an atmospheric electric field is also caused by continuous ionization of the near ground atmosphere and charged aerosol particles to which radon and its progeny are one of the significant sources. Radon produces up the order of 10^6 ion-pairs m^{-3} s^{-1} depending on exhaled the concentration. Also the electric field penetration into the ionosphere from the ground is higher. So it is obvious to directly relate this to the degree of radon emanation since its emission is more pronounced at night [65].

Amongst main factors relating earthquakes to the heterogeneity in radon concentration and atmospheric perturbation are radon variations with altitude under different mixing conditions such as day or night, the seasonal variation, wind speed and temperature gradient of soil-air boundary. The variation in air conductivity relative to seismicity is also pronounced due to the increase in ionization of planetary boundary layer (near earth surface) by radon and its progeny as shown in Figure 3.5. Also the study of variation of electric field of atmosphere and its relationship with radioactivity is significant, especially in understanding some of Earth's natural phenomena such as seismic studies [65].

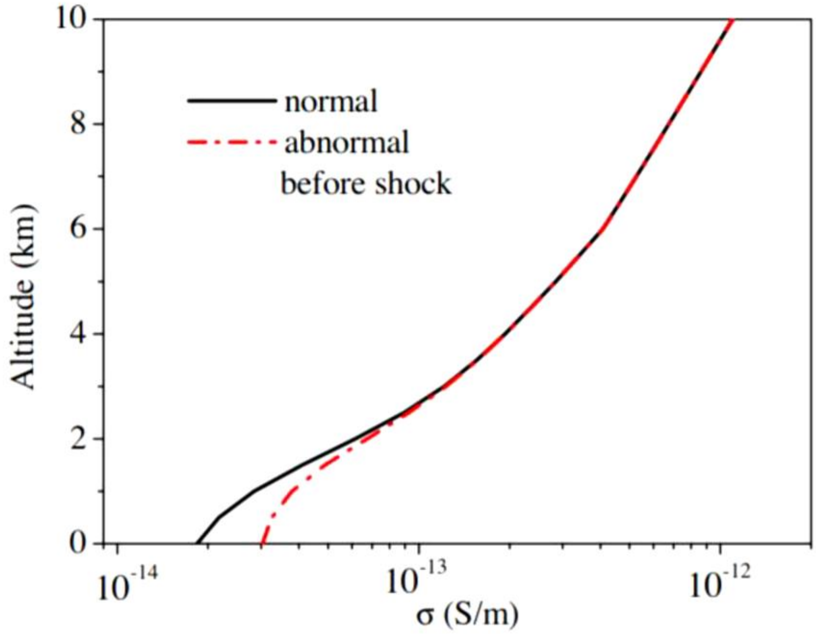

Figure 3.5. The variation of atmospheric conductivity with altitude affected by radon [65]

3.5. Study Area

As mentioned before, the presentation of the heavy isotopes ^{235}U, ^{238}U, ^{232}Th and their chains radionuclides on earth crust all over the world is varied depending on the local geological formation of that region. The main regional factors affecting the ^{222}Rn concentration, as gas, are geophysical, hydrogeological, geochemical phenomena (earthquakes, volcanic etc.) [6].

Also the ^{222}Rn migration is strongly affected by metrological factors. The weather conditions such as temperature, rain precipitation, wind speed and to some extent the pressure have greater effects on surface soil than the deeper parts [7].

Accordingly, the purpose of this section is to provide a brief overview to the topography, geology, and climate of Anatolia and Erzincan basin as study area.

3.5.1. Geographical Location

Erzincan governorate is located in the eastern region of Anatolia of Turkey, differentiating its name from its capital Erzincan district and city. Ekşisu town, where the ^{222}Rn concentrations had been examined, is located 11 km to the east of the Erzincan city center. It lies on the old Erzincan-Erzurum highway. Ekşisu is a recreational area and famous of natural mineral water comes out from the fountains. The total area of the province is 11,974 km^2 with a population of 236,034 in 2018 as shown in Figure 4.1 [66, 67].

The general shape of the Erzincan province is an irregular rectangle with longitude line from east to west of about 140 km. while from north to south it is about 20 km. The biggest cities are Erzincan close to the Cimin town. It is bordered by the provinces of Erzurum to the east, Baybur and Gümüşhane to the north, Sivas to the west, Malatya to the west-south and Tunceli to the south [68].

Erzincan province is divided into nine districts: Çayırlı, Erzincan, İliç, Kemah, Kemaliye, Otlukbeli, Refahiye, Tercan and Üzümlü. It has a strategic location since it is considered to be a point of joint among Erzurum and Istanbul. Its administrative map is shown in Figure 3.6.

As Erzincan city located to North Anatolian Fault (NAF), Turkey, it was destroyed severely and rebuilt twice, first after two destructive earthquakes, one of magnitude ML = 7.9 on December 27, 1939 and second the earthquake of march 13, 1992 of magnitude ML = 6.8 [69, 70].

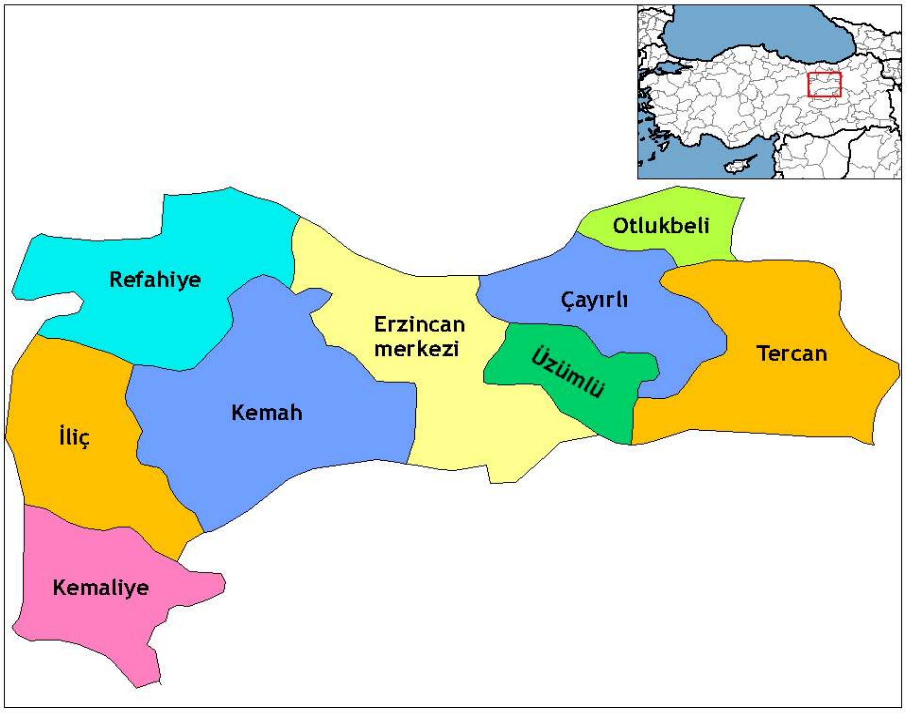

Figure 3.6. Administrative map of Erzincan [69]

3.5.2. Land

The town of Erzincan lies on the north bank of Kara River, and is one of the major branches feeding the Euphrates. It lies on a fertile plain, at an altitude of 1,200 meters above sea level, surrounded by snow-capped mountains. The field is situated entirely within the low folded region. Erzincan province lies within the two lines of Latitude and Longitude of 39°02′ - 40°05′

to the north and 38°16 - 40°45′ to the east, respectively. So it situates to the north of Equator in the northern Equinoctial area as given in Figure 3.7 [68].

3.5.3. Topography

One of the most tectonic and seismic events in Turkey is the upper crust of the Erzincan Basin and surrounding area. The Erzincan Basin lies inside a complex dock formed by the NW-SE bend on the right side of NAFZ and NE-SW, and then turns left to Ovacik Fault. It is historically the center of the largest events of the devastating earthquakes related to their major faults movements, which affected the city of Erzincan and other cities and villages around it, as shown in the lower part of Figure 3.7 [70].

The area within the Erzincan city is mostly covered by artificial surfaces and few croplands. In the farther areas by about 50 Km from Erzincan the land is covered by crops and grass, and going farthest to other districts by trees and sparse vegetation [68].

3.5.4. Geology

The geological properties of Turkey are very complex. Geologically it is classified into three major tectonic types: Pontides, Anatolides-Taurides and Arabian Platform. These three separate tectonic species, which in ancient times were surrounded by oceans, formed tectonic lines or regions along hidden oceans and created the present land [71].

The Pontides reflect the natural appreciation of the Laoretic and represent tectonic units in the Balkans and Caucasus as well as those in Central Europe. All had been situated north of New Tethys' northern branch. After this perimeter was completely closed, full production kept in Izmir, Ankara and Erzincan together, indicating the boundaries between Pontides and Anatolides-Taurides connected to the Arabian platform by sewing the Assyrians as shown in the upper part of Figure 3.7 [71].

The North Anatolian Fault Zone (NAFZ) is one of the world's most active seismically continental strike-slip fault zones. It stretches approximately 1200 km from Karlıova in the far east of Turkey and enters the far west Greek mainland as shown in the lower part of Figure 4.2 by green solid circles. [72].

There are some geological variations in the lower geological level of Erzincan area. It consists of Paleozoic rocks somewhat overlapped by the Miocene sequence with a thick carbon layer and the basin ends with Pliocene classic deposits. Several seismic tomography experiments in NAFZ showed that the Erzincan Basin is the largest unconsolidated sedimentary basin that magnifies ground movement during the Earthquake era. Some of these studies reported thickness of 2-4 km sedimentary basin included volcano-sedimentary rocks. [73,74].

The highlands (plateau) that characterized by low erosional surfaces are separated partially by broad valleys. The agricultural areas of the region are stabilized on the pyroclastic rocks and lacustrine sediments combined by volcanic ash [75].

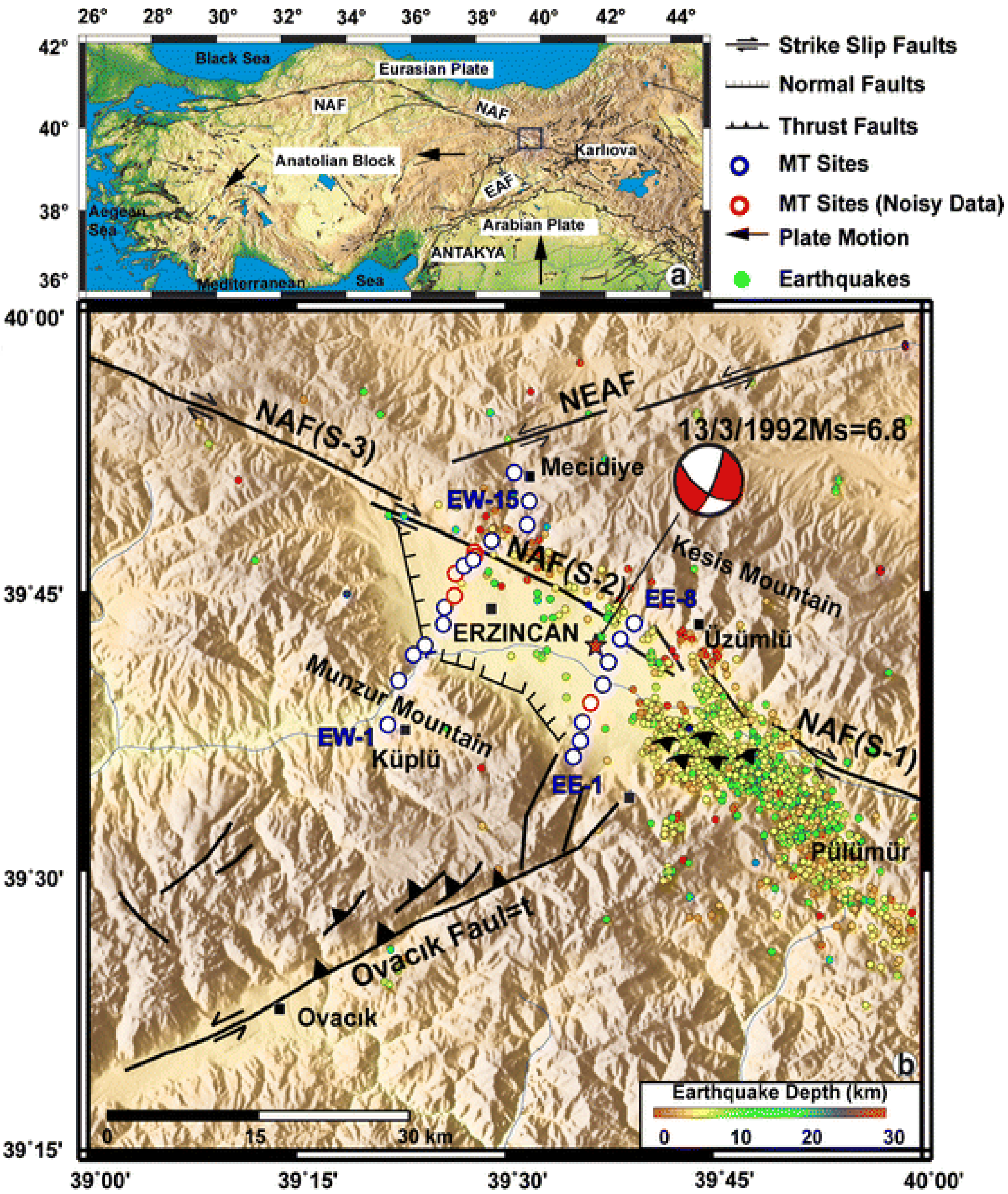

Figure 3.7. Lower**:** Topographic map of the Erzincan Basin surrounded by North Anatolian Fault NAFZ and Ovacik Fault OVF and Earthquake allocation [68]. Upper**:** expansion of NAFZ throughout Turkey and the study area symbolized by rectangle.

3.5.5. Climate

The climate of Erzincan is generally referred to as the continental and subtropical climate, which is generally characterized by broad diurnal and annual temperature ranges, very low relative humidity, cloudless summer months and the prevailing wind direction in the northwest according to Köppen climate classification. Its winter season is freezing and snowy while its summer is dry and warm. Also its spring season is the wettest [76, 66].

The Long Period monthly average maximum and minimum temperatures recorded is given in Figure 3.8. For a long period, the extremists temperature values recorded in Erzincan are; temperature drop to −32.5 °C in January 1950 as the lowest and jump to 40.6 °C in July 2000 as the highest. In the meanwhile the recorded maximum snow thickness is 74 cm in February 1950 [66, 76].

The monthly average rainfall as recorded in Long Period is given in Figure 3.9. The highest period of rainy days is 14.5 days in May, while the lowest of 2.6 days in August. From the figure, the wettest month of 54.5mm rain is May and the driest month (lowest rainfall) of 6.8 mm is August. It is worthwhile to mention the maximum sunshine month is July with an average of 10.6 hrs. and that of minimum is December with only 2.4 hrs. [76].

The humidity categorized by dew point in Erzincan, as measured by percentage of the concentration of water vapor in the air, remain very low and effectively constant 0% throughout to lower than 30% in July and August of summer season [68].

The average wind speed and direction is highly dependent on local topography and some other factors. In Erzincan the wind speed experiences mild seasonal variation yearly. Over the course of the year the average speed of the wind can be classified to three types according to the average wind speed and human comfort. These types are windier, windiest and calmer, which last different periods [68]:

1. Windier time; last approximately 3.2 months from end of January to the beginning of May with an average of 10.5 Km/hr.
2. Windiest time; may occur in the mid-march with an average hourly wind speed of 12.1 Km/hr.
3. Calmer time; it is the dominant and longest period in Erzincan, last for about 8.8 months, from beginning of May to the end of January and have leaser speed of about 9.0 Km/hr.

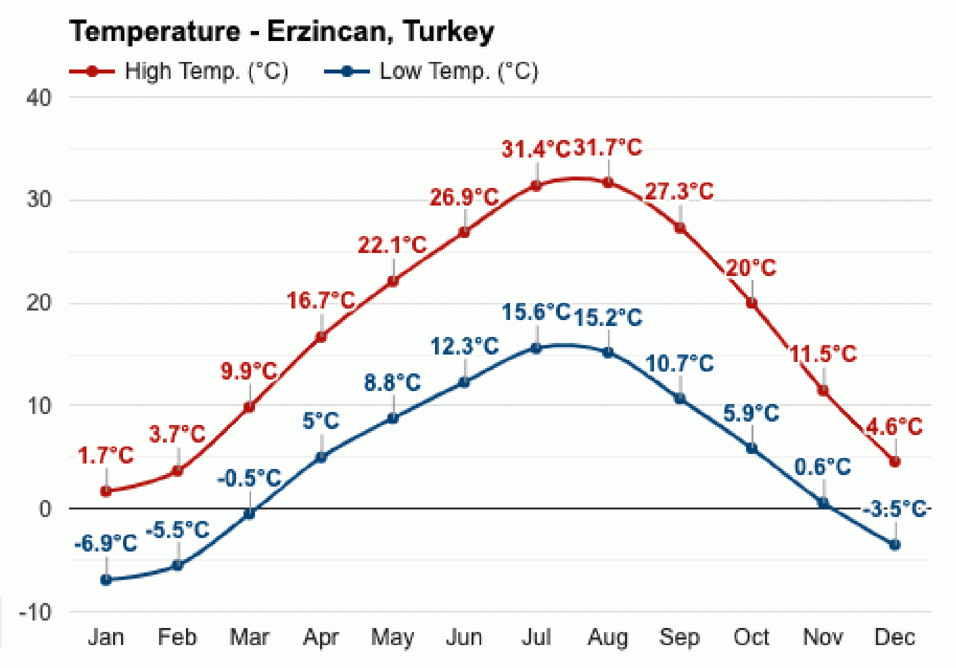

Figure 3.8. The monthly average high and low ttemperatures (°C) in Erzincan as recorded in Long Period [76]

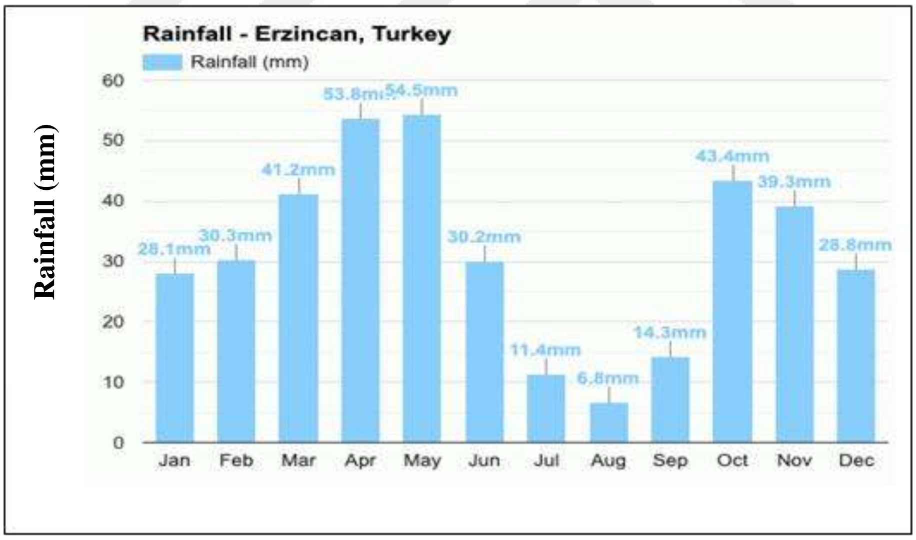

Figure 3.9. The monthly average rainfall of Erzincan accumulated over the course of year [76]

4. RESULTS AND DISCUSSION

This chapter focuses on the statistical analyses of ^{222}Rn concentration of soil obtained from seismic stations near the high seismically active location of Erzincan district, Ekşisu city of North Anatolian Fault Zone (NAFZ), Turkey. This region is classified as one of the continental fault zones with the most seismic activity in the world. Therefore, the impact of earthquake is dominant on the radon concentration significantly. While the other effects such as meteorological factors (temperature, humidity, pressure, etc…) can be considered non predominant or controlling compared to the impact of earthquakes.

2001 raw data of ^{222}Rn concentration from the soil of this site for duration of approximately three years are considered, Non-continuous or more precisely random records along March 11th 2007 to December 31th 2007 by 806 measurements, from January 1st 2008 to December 18th 2008 by 839 measurements, from February 4th 2009 to October 11th 2009 by 327 measurements and on February 9th 2010 by only 30 measurements. All data within short measuring periods of 15 minutes are considered. ^{222}Rn concentrations are studied according to time series analysis.

4.1. Descriptive Statistical Information

From the characteristics of time series described in chapter 3, the radon observations are irregular, random and unpredictable data in its variation with time or in other words it is chaotic. This is because ^{222}Rn concentration is strongly affected by earthquakes and to some extent affected by meteorological conditions of the region.

Despite of the non-stationarity behavior of the time series it is appropriate to qualitatively summarize the time series. By assuming the time series is stationary then all its statistical observations such as mean, variance, standard deviation, etc. have to be constant with time. The fundamental statistical properties of 2001 observations time series of Erzincan region as have been calculated by EXCEL software are given in Table 4.1.

Table 4.1. Fundamental statistical analysis for ^{222}Rn observations

Statistical information	^{222}Rn (Bqkm^{-3})
No. of observation	2002
Min. concentration	0
Max. concentration	99
mean value	23.2
Median value	18
Std. Dev. σ	16.4
Variance	268.3
95% Confidence Interval	0.60

4.2. Radon's Time Series

Time series of radon observations is a random data variation in a time series. It shows non-stationarity behavior as it characterized by trend patterns and irregularity because of unpredictable events occurred in a seismic region. MATLAB software is applied to analyze the Erzincan radon data. This Code will demonstrate how to implement ARIMA model and Monte-Carlo simulations on radon Time series data [48].

4.2.1. Impact of earthquakes

Before analyzing the non-stationarity and non-linearity of ^{222}Rn concentration time series, it is necessary to show the impact of earthquakes occurred in and around this high seismically active region during the period of the study. Earthquakes have a tremendous impact on the geological formations of the region through the imbalance of rock and dust layers, and accordingly on the transmission of radon and thus an increase in radon concentrations.

About 36 micro-earthquakes of magnitude (ML, 3.4 to 5) in the Richter local scale strike the region during the three mentioned years, as shown in Figure 4.1. The range of the depth of the earthquakes epicenters to the Ekşisu regional station are about 2.3 - 10 km, of average 5 km, and the range of distance of about 2 – 50 km. In addition, Figure 4.1 shows the general physical change in radon behavior via plotting the moving average curve.

The moving average is one of statistical analysis method that creates a secondary series of the averages from subsequent subsets. Its curve represents a trend of data within the full dataset time series by moving forward subsets of data starting from the first to the last subset. The second statistical tool to forecast event of the general time-series trends is the Least Square method through the extrapolation of the fitted straight line.

Figure 4.1, adopted from EXCEL, provide some remarkable information on the effect of earthquakes on the ^{222}Rn anomalies in the soil. For instance, closer distance of earthquake the sharper increase in radon concentration as in (ML 4.7 and 3.6) happened in Erzincan, September 17th 2008. Also, the higher magnitude of earthquake gives the higher concentration as in (ML 5.0) in Erzincan, July 30th 2009. It is obvious the depth of the earthquake epicenter has also a negative impact on the ^{222}Rn concentration. From the moving average curve, it is noticeable the graduate increases of ^{222}Rn concentration due to some far and lower magnitudes earthquakes prior the two peaks at 9/17/2008 and 8/24/2009 due the two earthquakes happened in Erzincan at 9/17/2008 (ML 4.7) and 7/30/2009 (ML 5) respectively.

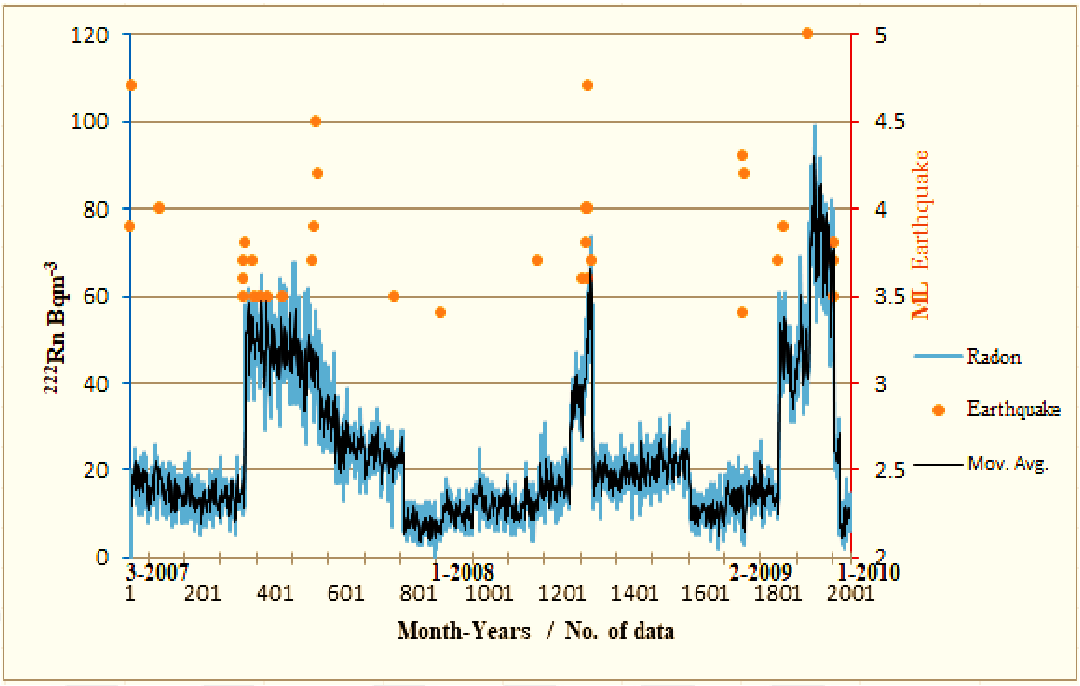

Figure 4.1. Time series of ^{222}Rn concentration, moving average and Earthquakes of the raw data

4.2.2. Maximum daily time series

Because the obtained ^{222}Rn concentration data, as mentioned before, are somehow random and not continues in dates (within short measuring periods of 15 minutes), the calculated maximum values day by day of ^{222}Rn concentration is adopted to examine the physical behavior of a time series. Also this may be helpful in forecasting the short and long term macro-earthquake prediction. The daily maximum values omit the variation of meteorological conditions during the day and consequently may signify the relationships between the earthquake magnitude (ML) and ^{222}Rn concentration levels (Bqkm^{-3}). The resultant calculated maximum daily radon levels and earthquake magnitudes are given in Table 4.2.

Table 4.2. The calculated maximum daily radon levels and earthquake magnitudes

Date m/d/year	**Time** Days	Max-**Rn** **Bqkm^{-3}**	**Earthq** **ML**	**Date** m/d/year	**Time** Days	**Max-Rn** **Bqk^{-3}**	**Earthq** ML	**Date** m/d/year	**Time** Days	**Max-Rn** **Bqkm^{-3}**	**Earthq** ML
10/28/2007	1		4.2	6/27/2008	244		4	2/17/2009	479	19	
11/27/2007	31	35		6/29/2008	246	61		2/18/2009	480	23	
11/28/2007	32	39		7/12/2008	259		4	3/11/2009	501		4.3
11/29/2007	33	34		8/12/2008	290		3.8	4/15/2009	536		4.2
12/1/2007	65	13		9/17/2008	326		4.7	3/25/2009	515	11	
1/2/2008	67	13	3.4	9/22/2008	331	74		4/25/2009	546	27	
2/14/2008	110	18		10/3/2008	342		3.7	4/26/2009	547	21	
2/15/2008	111	16		10/21/2008	360	26		6/13/2009	595		3.7
2/26/2008	122	25		10/22/2008	361	28		7/7/2009	619	61	
2/28/2008	124	17		10/23/2008	362	31		7/8/2009	620	61	
3/17/2008	142	22		11/10/2008	381	20		7/12/2009	624	53	
4/17/2008	173		3.6	11/11/2008	381	25		7/23/2009	635	69	
4/28/2008	184	31		11/14/2008	384	33		7/27/2009	639	58	
4/29/2008	185	25		11/15/2008	385	31		7/30/2009	642	71	5
6/21/2008	238	47		12/17/2008	417	16		8/24/2009	667	99	
6/22/2008	239		3.6	12/18/2008	418	19		8/27/2009	670	87	
6/24/2008	241		3.8	2/4/2009	466	14		9/18/2009	692		3.7

Figure 4.2 displays time series provided by the maximum daily value of ^{222}Rn concentration as a function of time in days, starting from the minimum concentration reached at 12/31/2007 up to the last observation day 9/18/2009. The figure also presents the curve of moving averages and the least squares fitting to serve as forecasting tools of expected earthquake in future. In addition, an application of least square fitting to the magnitude level ML of a group of earthquakes in the same period is shown in Figure 4.2.

It is noticeable, from Figure 4.2, the graduate increases of ^{222}Rn concentration in the soil after four subsequent earthquakes started from 1/2/2008 (day 67) to 6/27/2008 (day 244) generated anomalies and rising in ^{222}Rn levels in the soil after 2 days at 6/29/2008, refer to Table 4.2. This dramatic change in radon concentration is clear in the moving average curve given in Figure 4.2. The dramatic anomalies in concentrations requires the use of nonlinear analysis

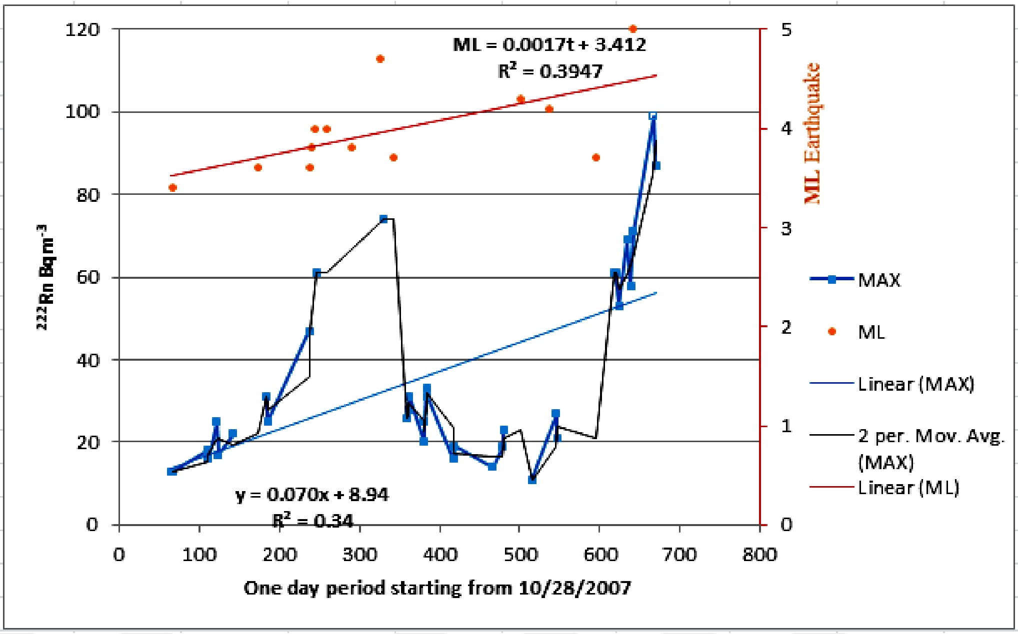

Figure 4.2. Daily ^{222}Rn time series, moving averages and Earthquakes and least square fitting on both

Applying the least square fitting to the daily maximum values of radon levels and the earthquake (ML) showed the following correlations:

For radon concentration Rn;

$$Rn = 0.070.t + 8.94 \quad R^2 = 0.34 \tag{4.1}$$

and for earthquake magnitude ML;

$$ML = 0.0017.t + 3.412 \quad R^2 = 0.395 \tag{4.2}$$

where, t is the time in days.

A macro-earthquake of ML = 5.4 happened in Elazig-İçme, on 6/23/2011 having focal depth of 5.7 km and about 200 km far from Erzincan is taken as an example to improve the above correlations as reported in [12]. 6/23/2011 accounts 1335 days from the first day considered for the moving average and least square forecasting at 10/28/2007. The results obtained by Equations 4.1 and 4.2 gives Rn = 47 Bqkm^{-3} and ML = 5.67 respectively. Even the radon concentration underestimates the reported value, these results show encouragement agreement.

4.3. MATLAB Analysis

In the present work MATLAB software package is adopted to analyze the Erzincan radon data [47, 48]. This Code demonstrates the implementation of ARIMA and Monte-Carlo on radon Time series data. The full software is given in appendix-1.

4.3.1. Sample Autocorrelation Function

Radon data is divided into Train and test for forecasting purpose. The training data named Train has 1900 observation points while the test has 100 points. As a total these data make a total of 2000 observation for the radon data from 2007 to early 2010. It should be mentioned that these data have some missing observations.

Radon time series of Erzincan, located to North Anatolian Fault (NAF), Turkey, is plotted in Figure 4.3 as adopted from the code, where ARIMA model was implemented on it. As show in Figure 4.1, the vertical axis is soil radon concentration in $Bqkm^{-3}$ and the horizontal axis is the time with intervals of 15 minutes for each radon data measured (From March 2007-February 2010).

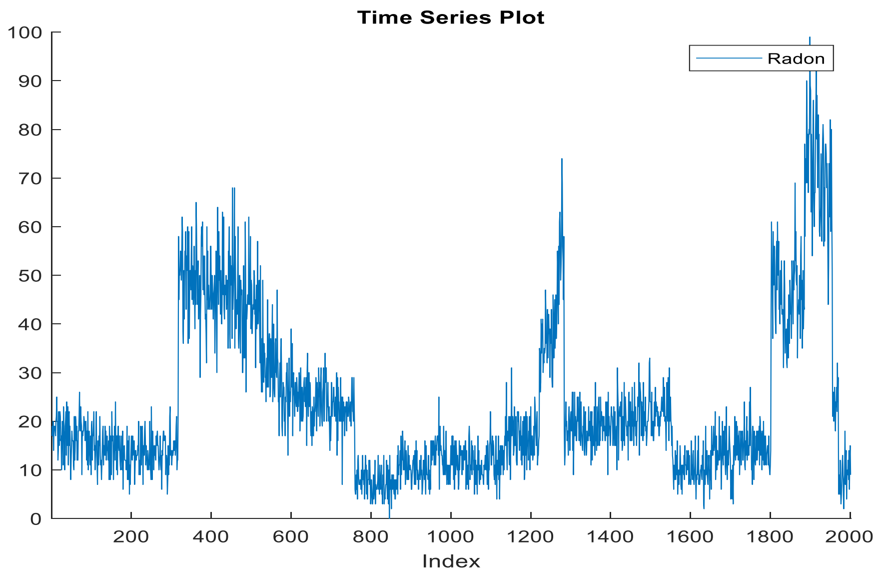

Figure 4.3. Time series plot of radon; Train1

As mentioned in Chapter 3.2.2, plotting the Autocorrelation function ACF and Partial Autocorrelation Function PACF of the data can help determining the value of p and q as well as whether the data needs differencing or not, i.e. the existence of trend. The plots in Figures 4.4 (a) and (b) shows ACF and PACF sense of stationarity the Radon-Train data respectively.

Figure 4.4 (a) shows the ACF plotting to identify number of Lags crossing the confidence interval, which represent the value of (*q*) in ARIMA. Although three lags cross the confidence (blue) line it can be seen that the only one significant lag cross the confidence bound at position 1.

The PACF in Figure 4.4 (b) is geometrically declining. Therefore the value of (*p*) can be any, and the best value is (p = 1). Accordingly the expected combination can start with ARIMA (1,0,1). But one more criteria in choosing a better model combination is the AIC and BIC.

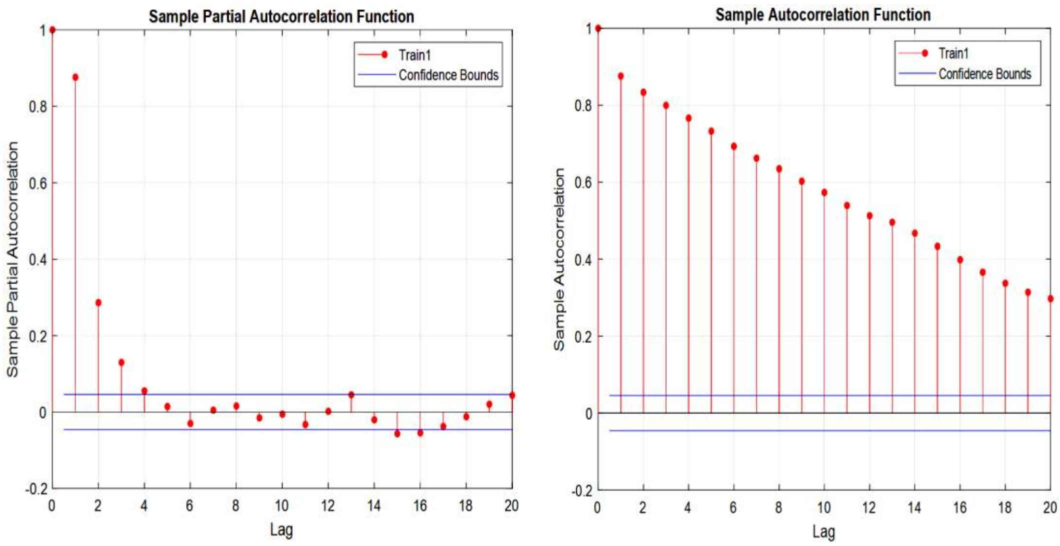

(a) **(b)**

Figure 4.4. (a) Sample ACF of Train1, (b) Sample PACF of Train1

4.3.2. Augmented Dickey-Fuller Test

The Dickey fuller's unit root stationarity test has been applied [43, 44]. The test is carried out on first 20 lags of the data.

Null Hypothesis: Train1 contains a unit root

$$y_t = c + \delta t + \phi y_{t-1} + \beta_1 \Delta y_{t-1} + \cdots + \beta_p \Delta y_{t-p} + \varepsilon_t \qquad (4.3)$$
$$H_0 : \Phi = 1 \qquad H_a : \Phi < 1$$

Table 4.3. Test Parameters

Lags	Model	Test Statistic	Significance Level
20	AR	t1	0.05

Table 4.4. Test Results

Null Rejected	P-Value	Test Statistic	Critical Value
true	0.0037442	-2.9556	-1.9416

The p-value in Table 4.4 is 0.0037442 with a significance level of 0.05, suggesting that the null hypothesis is agreed. Now based on the ACF and PACF plots in Figure 4.4 (a) and (b) the best possible ARIMA(*p*,*d*,*q*) is chosen *p* = 1 for AR(*p*) model and *q* = 1 for MA(*q*) with no differencing, i.e. *d*=0 for I. Accordingly, ARIMA(1,0,1) is used.

4.3.3. ARIMA(1,0,1) Model (Gaussian distribution) (ARIMA_Train1)

Autoregressive integrated moving average model of time series Train1 with the following equation:

$$(1 - \phi_1 L) y_t = c + (1 + \theta_1 L) \varepsilon_t \tag{5.4}$$

According to the obtained results and shown in Table 4.5 and 4.6, the model ARIMA(1,0,1) is reasonable, and has less than significance (α = 0.05) P-value for both AR(1) and MA(1). The model fit plot is shown in Figure 4.1.

Table 4.5. Estimation Results

Parameter	Value	Standard Error	T Statistic	P Value
Constant	1.013	0.25377	3.9919	6.5534e-05
AR{1}	0.95552	0.0066097	144.5617	0
MA{1}	-0.38176	0.014238	-26.8118	2.3517e-158
Variance	56.4911	0.81612	69.2189	0

Table 4.6. Goodness of Fit

AIC	13064.7268
BIC	13086.9231

4.3.4. Residual diagnostics

To further explore the power of the model, it will be good to visualize the residuals which can be seen in Figure 4.5 the residuals seem to fluctuate around the mean.

However, to support this we need to look further to Figure 4.6 (a), where the histogram indicating normality, i.e. that the residual distribution is centered on the mean. And this is implied in Figure 4.6 (b) with the quantiles for both residuals and that of the normal distribution merge, with only few deviations at the tail. With this we can assume that the ARIMA(1,0,1) model fits reasonably. A complement to this is seen in Figure 4.6 (c), the autocorrelation function did not have any significant lag.

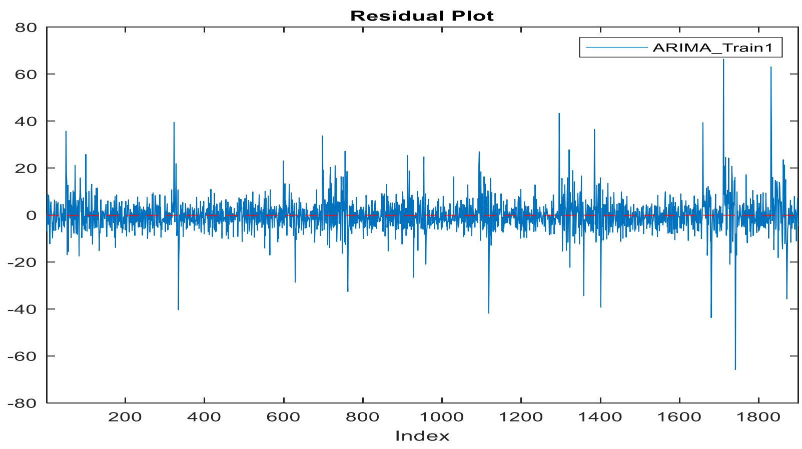

Figure 4.5. Plot of the residuals of model ARIMA_Train1

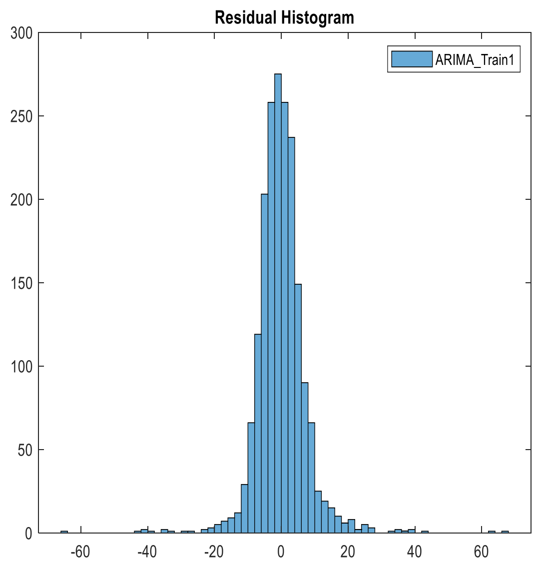

(a)

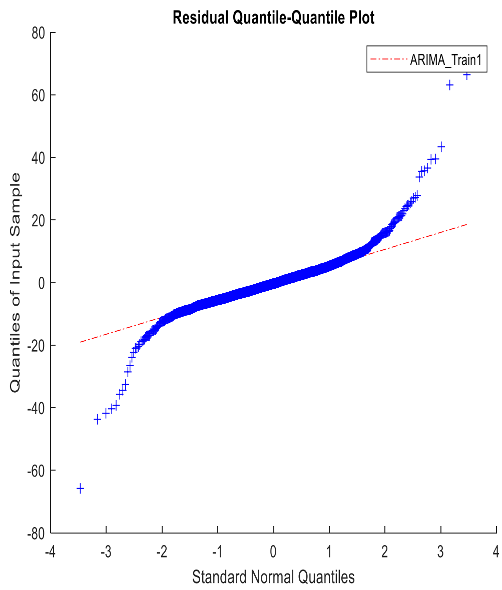

(b)

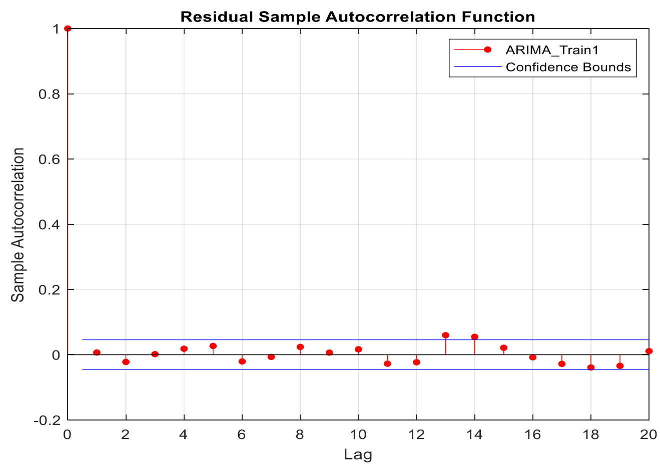

(c)

Figure 4.6. (a) Histogram of the residuals, (b) Quantile-quantile plot of the residuals, and (c) Autocorrelation function of residuals

4.4. Earthquakes verses Radon, Meteorological Parameters and TEC

The relationships between radon concentration, meteorological Parameters (atmospheric pressure and atmospheric and 5 cm above soil temperature), and Earthquakes within the period of the study are given in Figure 4.7, while the behavior of atmospheric Total Electron Content (TEC) related to earthquakes within the period of two macro earthquakes ML = 4.7 occurred in September 2008 and ML = 5.0 in July 2009 is shown in Figure 4.8 (a) and (b) respectively. These relationships are really a big task to be explored and plague and strain many researchers over the decades.

As it has been proven that the impact of earthquake is dominant on the radon concentration significantly. A linear relation between mean soil temperature and radon activity by some researchers a reverse proportionality of radon level with the rest meteorological parameters [13]. It is clear from Figure 4.7 that the most and highest earthquakes recorded in hot summer season and high pressure. This analogy with the maximum ^{222}Rn concentrations recorded in summer season and minimum in cold winter seasons.

Atmospheric Total Electron Content (TEC) in TECU unit where 1 TECU = 10^{16} electrons/m², which represents the density of the electron columnar number, is an important descriptive amount for the Earth's ionosphere. Figure 4.8 (a) shows an increase in TEC after the earthquake. While Figure 4.8 (b) shows a small decrease in TEC before earthquake. Earthquake prediction monitoring and analysis employ a regular inspection ionosphere TEC differentiated from the GPS receiver global positioning system.

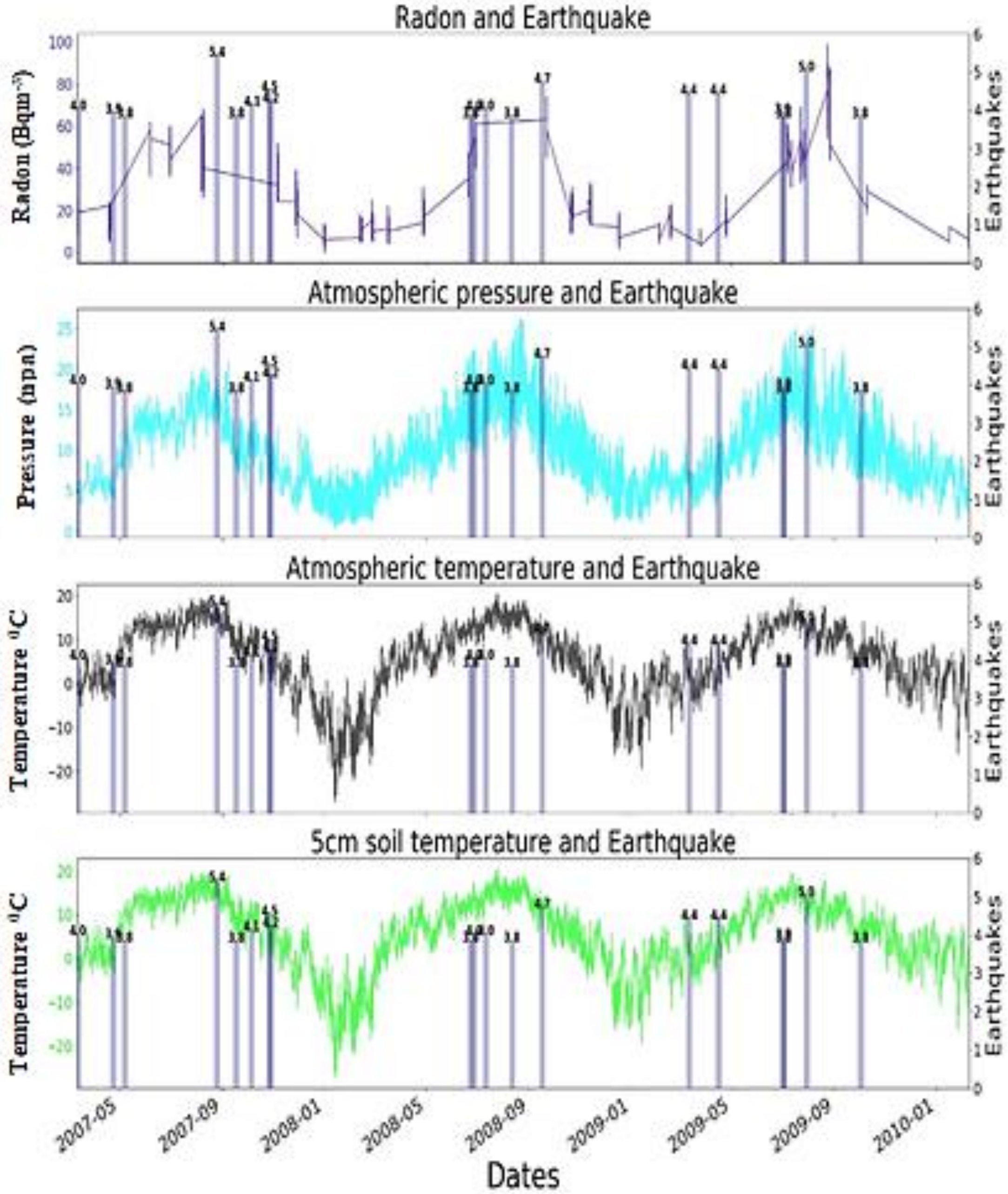

Figure 4.7. Relationships between radon concentration, meteorological Parameters, atmospheric total electron content TEC and Earthquakes

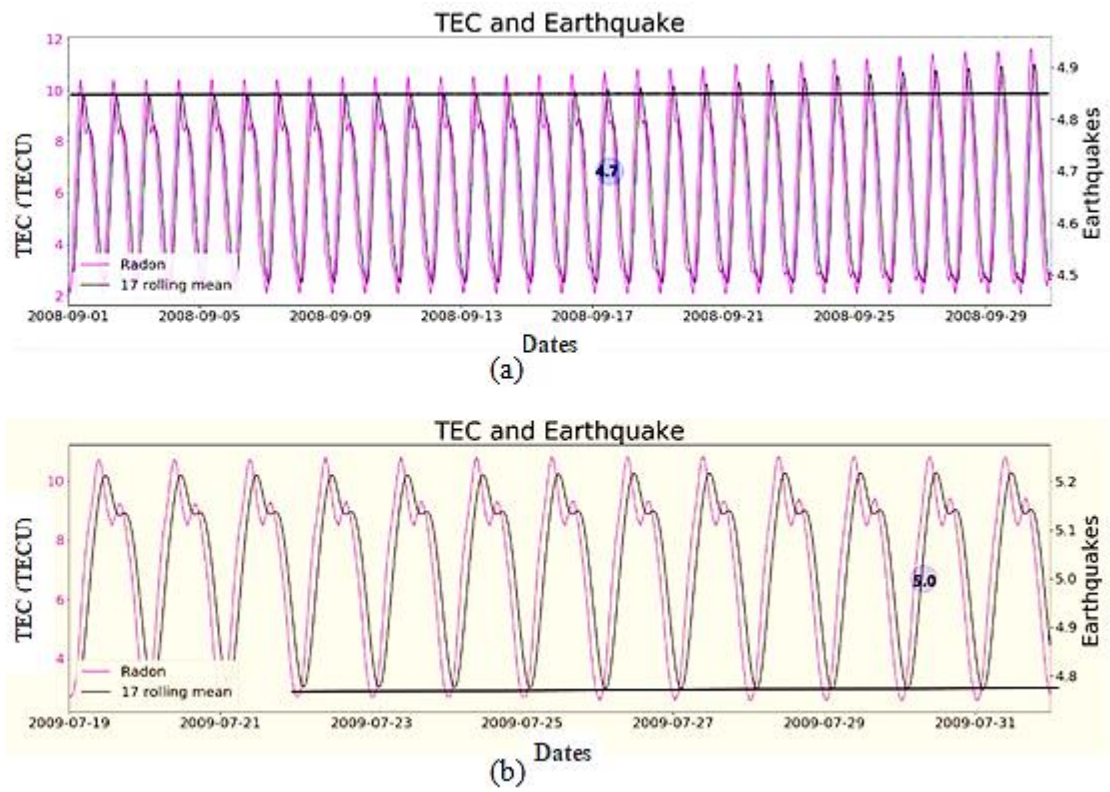

Figure 4.8. Atmospheric Total Electron Content (TEC) relationship with earthquakes

4.5. Model forecast

A dynamic modeling is used to analyze time series data. The main goal, in analyzing the time series data, is to forecast and predict the future values of the chain from the understanding of the past. Different time series forecasting Dates ' 's have been developed for the purpose of statistical analysis. Among many stochastic models frequently used are the Auto-Regressive Integrated Moving Average (ARIMA) and Monte-Carlo simulations to forecast time series observations that build in MATLAB software package. In addition, EXCEL software is helpful.

4.5.1. Model forecast: ARIMA simulation

Having the model fit the data; it would be good to see more by looking at the 100-time step forecast as shown in Figure 4.9. The forecast seems good from the first few steps, and then gets off where radon anomaly spikes for a little further steps. Then it gets back to track. This forecast is connected to the impact of earthquakes occurred at the spike points as shown in Figure 4.1.

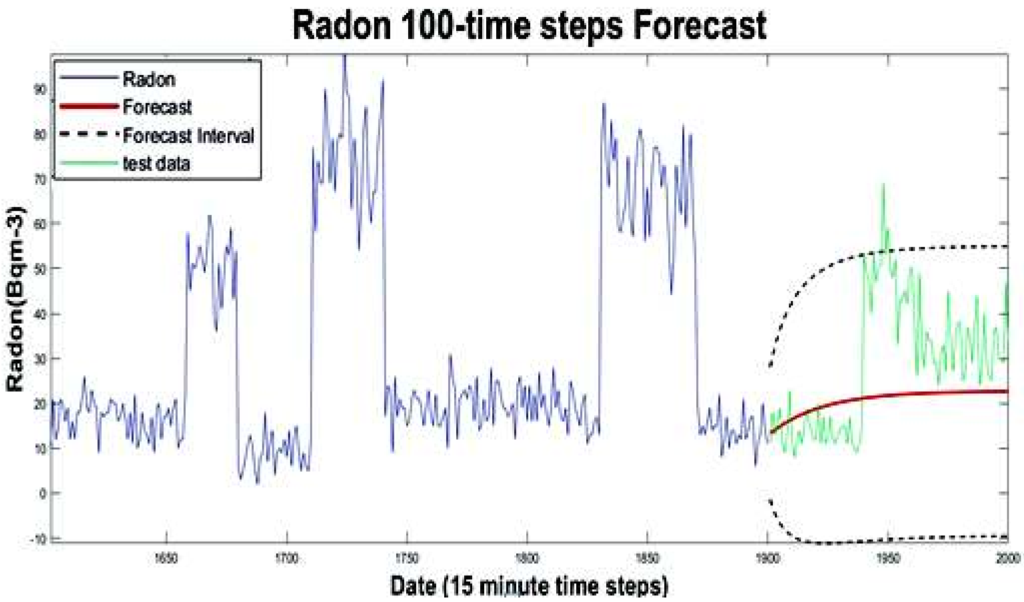

Figure 4.9. 100-time step forecast for Radon-ARIMA(1,0,1) model

4.5.2. Model forecast: Monte-Carlo simulation

To improve the model, Monte-Carlo simulation for 7 different paths is shown in Figure 4.10. It is seen that some of the simulated paths have overestimated while others underestimated. The mean Monte-Carlo path is indicated with dashed black line. The Monte-Carlo results would estimate better when the number of paths are increased. In each case the, results seem reasonable.

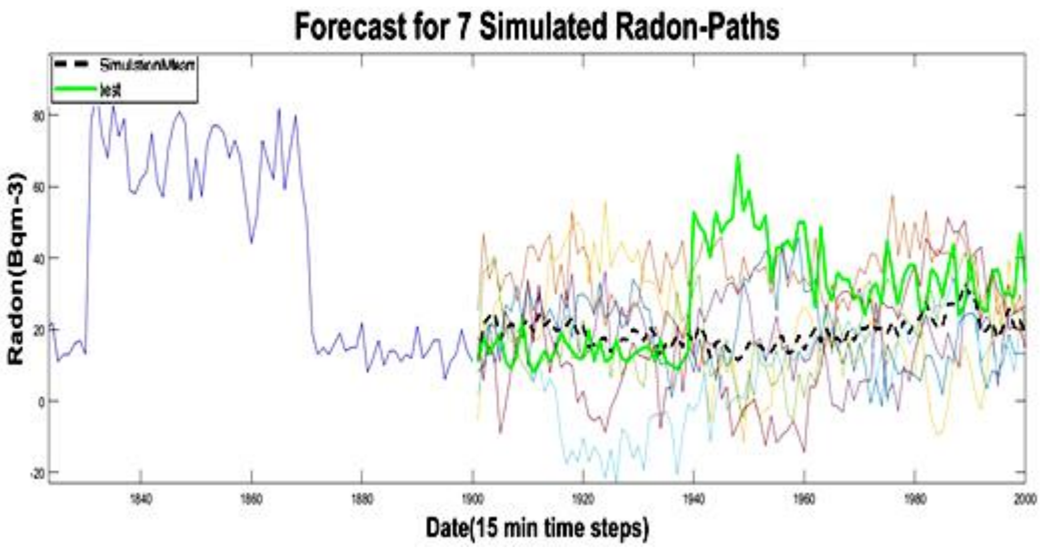

Figure 4.10. A forecast for 7 Monte-Carlo simulation paths

5. CONCLUSION

From the statistical analysis by different methodologies and results obtained, it can be concluded that:

1. The large number of earthquakes occurred in Erzincan of North Anatolian Fault Zone (NAFZ) during the period of this work shows way this region is classified as one of the most seismically active continental strike-slip fault zones in the world. Therefore, the impact of earthquake is dominant on the radon concentration significantly. While the other effects such as meteorological factors (temperature, humidity, pressure, etc…) can be considered non predominant or controlling compared to the impact of earthquakes.
2. From the characteristics of time series, the radon observations are irregular, random and unpredictable data in its variation with time or in other words it is chaotic. This is because ^{222}Rn concentration is strongly affected by earthquakes and to some extent affected by TEC and meteorological conditions of the region.
3. A closer distance of earthquake epicenter the sharper increase in radon concentration, also the magnitude of earthquake has a positive impact. The depth of the earthquake epicenter has a negative impact on the ^{222}Rn concentration.
4. The dramatic anomaly of radon concentrations in the moving average curve after each earthquake necessitates the use of nonlinear time series analysis to extract important information about the behavior of the dynamic system.
5. The least square fitting to the daily maximum values of radon levels and the earthquake (ML) showed acceptable prediction of macro-earthquake. This may be because the daily maximum values omit the variation of meteorological conditions during the day and consequently may signify their relationships but still the seasonal variations have to be investigated.
6. ARIMA simulation shows good forecast from the first few steps, and then gets off where radon anomaly spikes for a little further steps. Then it gets back to track and this might be due to the impact of earthquakes occurred at the spike points.
7. Monte-Carlo simulation for 7 different paths shows some of the simulated paths have overestimated while others underestimated. In general, the results seem reasonable. The forecast might be better if the numbers of paths are increased.
8. ^{222}Rn's 3.82-day half-life is equivalent to that of primary atmospheric contaminants and the synoptic time scale. This half-life is long enough compared to typical turbulent time

scales (~1 h); therefore, it is considered to be well suited for tracing of air transport in the atmospheric boundary layer (ABL) and over land studies.

9. Previous studies show that near ground atmospheric layers behave with large vertical gradients of temperature, wind velocity and humidity. Atmospheric electric field or electricity near ground atmospheric layers depends on many factors or sources. Among such sources are the turbulence in the planetary boundary layer, cloudiness, air pollution, aerosols of different origin such as the volcanic eruptions and natural radon and daughter products degassing from the Earth's crust.
10. Among the reported results, the emanation of radon from the earth crust drastically changes the parameters of the near ground layer. This emanation can change the value of the electric field within the layer by several times up to the reverse sign of the electrode effect. Ionization effectiveness of the ^{222}Rn and its progenies could be up to 10 times larger than that of the cosmic rays which can affect the thunderstorm activity; in addition, the surface roughness also has an effect on the near ground electric field variability.
11. Earthquake prediction starts by combining ground and satellite observations of complex space-borne systems and earthquake precursors electromagnetic and ionosphere precursors with those still under construction.
12. It is clear from the radon time series that closer distance of earthquake the sharper increase in radon concentration as in (ML 4.7 and 3.6) happened in Erzincan, September 17th 2008. Also, the higher magnitude of earthquake gives the higher concentration as in (ML 5.0) in Erzincan, July 30th 2009. It is obvious the depth of the earthquake epicenter has a negative impact on the ^{222}Rn concentration.

Furthermore suggestions for Future Studies based on the data and the obtained results in present study can be summarized as below:

1. Since the analysis of radon time series within short measuring periods of 15 minutes along years is tedious and this could strongly eliminate the effect of meteorological factors. An analysis of seasonal variations of ^{222}Rn concentration might be adopted by fitting a sinusoid or any dynamic model to the atmospheric daily maximum or minimum radon data. In this case the radon variations will match the variation at the top mixing layer and establish normal seasonal pattern.
2. Mapping the radon exhalation rate from soil is essential in forecasting earthquakes, specifically in the highly effective seismic regions. Several maps have been reported nationally all over the world. These maps will be useful in evaluating the mechanism for the emanation, transport and exhalation of radon from soil.

3. Study the transport of radon via atmospheric dynamics through coupling between atmospheric layers in conjunction with one or preferably an ensemble of observations by using nonlinear models such as global models, quasi-static model…etc.

REFERENCES

[1] Alias, M., Hamzah, Z., Saat, A., Omar, M., & Wood, A. K. (2008). An assessment of absorbed dose and radiation hazard index from natural radioactivity. *Malaysian Journal of Analytical Sciences*, *12*(1), 195-204.

[2] Vesterbacka, P. (2005). 238U–series radionuclides in Finnish groundwater-based drinking water and effective doses.

[3] Okeyode, I. C., & Moshood, I. A. (2010). Elemental compositions of the soil of Ogun-Osun river basins development authority headquaters, Ogun-state, Nigeria. *Indian Journal of Science and Technology*, *3*(3).

[4] Abu-Zeid, H., El-Nagar, T., Awad, S., Abd-El Maksoud, T. M., & Nada, A. (2009). Distribution of Radionuclides in Soil Samples from a Petrified Wood Forest in El-Qattamia, Cairo, Egypt. *Applied Radiation and Isotopes–UK,(2009), 67: 643-649*.

[5] Moran-Hunter, C. (2008). Transfer of radionuclides from Soil to Vegetation in Selected Irish Ecosystems", Institute of Technology Sligo.

[6] National Research Council. (2008). *Radiation source use and replacement: abbreviated version*. National Academies Press.

[7] Zoran, M., Savastru, R., & Savastru, D. (2012). Ground based radon (222Rn) observations in Bucharest, Romania and their application to geophysics. *Journal of Radioanalytical and Nuclear Chemistry*, *293*(3), 877-888.

[8] Zeeb, H. (Ed.). (2009). *WHO handbook on indoor radon: a public health perspective*. World Health Organization.

[9] Fischer, D. (1997). History of the International Atomic Energy Agency. The First Forty Years, Vienna, IAEA.

[10] Wilkening, M. (1990). *Radon in the Environment*. Elsevier.

[11] Kamişlioğlu, M., & Külahci, F. (2016). Chaotic behavior of soil Radon gas and applications. *Acta Geophysica*, *64*(5), 1563-1592.

[12] Külahcı, F., & Çiçek, Ş. (2015). Time-series analysis of water and soil radon anomalies to identify micro–macro-earthquakes. *Arabian Journal of Geosciences*, *8*(7), 5239-5246.

[13] Yakut, H., Tabar, E., Yıldırım, E., Zenginerler, Z., Ertugral, F., & Demirci, N. (2017). Soil gas radon measurement around fault lines on the western section of the North Anatolian fault zone in Turkey. *Radiation protection dosimetry*, *173*(4), 405-413.

[14] Aktar, M., Dorbath, C., & Arpat, E. (2004). The seismic velocity and fault structure of the Erzincan basin, Turkey, using local earthquake tomography. *Geophysical Journal International*, *156*(3), 497-505.

[15] Hayashi, K., Yasuoka, Y., Nagahama, H., Muto, J., Ishikawa, T., Omori, Y., ... & Mukai, T. (2015). Normal seasonal variations for atmospheric radon concentration: a sinusoidal model. *Journal of environmental radioactivity*, *139*, 149-153.

[16] Hafez, Y. I., & Awad, E. S. (2016). Finite element modeling of radon distribution in natural soils of different geophysical regions. *Cogent Physics*, *3*(1), 1254859.

[17] Zhuo, W., Iida, T., & Furukawa, M. (2006). Modeling radon flux density from the earth's surface. *Journal of nuclear science and technology*, *43*(4), 479-482.

[18] Mansour, H. H., per Khdar, S., Abdulla, H. Y., Muhamad, N. Q., Othman, M. M., & Qader, S. (2005). Measurement of indoor radon levels in Erbil capital by using solid state nuclear track detectors. *Radiation measurements*, *40*(2-6), 544-547.

[19] Pulinets, S. A., Alekseev, V. A., Boyarchuk, K. A., Hegai, V. V., & Depuev, V. K. (1999). Radon and ionosphere monitoring as a means for strong earthquakes forecast. *Il nuovo cimento C*, *22*(3-4), 621-626.

[20] Abdullah, K. (2017). *Fundamentals in IN Nuclear Physics* (p. 259). Noor Publishing.

[21] Alpen, E. L. (1997). *Radiation biophysics*. Academic press.

[22] Peña, A. M. (2011). Radioactive Air Sampling Methods. *Health Physics*, *101*(6), 761.

[23] Zhang, K., Feichter, J., Kazil, J., Wan, H., Zhuo, W., Griffiths, A. D., ... & Yver, C. (2011). Radon activity in the lower troposphere and its impact on ionization rate: a global estimate using different radon emissions. *Atmospheric Chemistry and Physics*, *11*(15), 7817-7838.

[24] Ball, T. K., Cameron, D. G., Colman, T. B., & Roberts, P. D. (1991). Behaviour of radon in the geological environment: a review. *Quarterly Journal of Engineering Geology and Hydrogeology*, *24*(2), 169-182.

[25] Nazaroff, W. W. (1992). Radon transport from soil to air. *Reviews of geophysics*, *30*(2), 137-160.

[26] Wilkening, M. (1990). Studies in Environmente. Elsevier.

[27] https://en.wikipedia.org/w/index.php?title=Radon&oldid=888607160 [Accessed: 21-Mar-2019].

[28] Wilkening, M. (1990). *Source of Radon in Rocks and Soils*. Elsevier, vol. 40.

[29] Wilkening, M. (1990). Radon Decay Products in the Atmosphere", in *Studies in Environmental Science*, Ed. Elsevier B.V., pp. 81–90.

[30] Mehta, N., & Kocar, B. D. (2018). Deciphering and Predicting Microscale Controls on Radon Production in Soils, Sediments and Rock. *Soil Systems*, *2*(2), 30.

[31] Sakoda, A., Ishimori, Y., & Yamaoka, K. (2011). A comprehensive review of radon emanation measurements for mineral, rock, soil, mill tailing and fly ash. *Applied Radiation and Isotopes*, *69*(10), 1422-1435.

[32] Richon, P., Bernard, P., Labed, V., Sabroux, J. C., Beneïto, A., Lucius, D., ... & Robe, M. C. (2007). Results of monitoring 222Rn in soil gas of the Gulf of Corinth region, Greece. *Radiation measurements*, *42*(1), 87-93.

[33] Chowdhury, S., Deb, A., Nurujjaman, M., & Barman, C. (2017). Identification of pre-seismic anomalies of soil radon-222 signal using Hilbert–Huang transform. *Natural Hazards*, *87*(3), 1587-1606.

[34] Ramola, R. C., Prasad, Y., Prasad, G., Kumar, S., & Choubey, V. M. (2008). Soil-gas radon as seismotectonic indicator in Garhwal Himalaya. *Applied Radiation and Isotopes*, *66*(10), 1523-1530.

[35] NCRP, M. (1987). NCRP Report No. 93, Ionizing Radiation Exposure of the Population of the United States. *Bethesda, MD: NCRP*.

[36] Ajayi, K. M., Shahbazi, K., Tukkaraja, P., & Katzenstein, K. (2018). A discrete model for prediction of radon flux from fractured rocks. *Journal of Rock Mechanics and Geotechnical Engineering*, *10*(5), 879-892.

[37] Samet, J. M. (1989). Radon and lung cancer. *JNCI: Journal of the National Cancer Institute*, *81*(10), 745-758.

[38] Al-Zoughool, M., & Krewski, D. (2009). Health effects of radon: a review of the literature. *International journal of radiation biology*, *85*(1), 57-69.

[39] Vaupotič, J., Smrekar, N., & Žunić, Z. S. (2017). Comparison of radon doses based on different radon monitoring approaches. *Journal of environmental radioactivity*, *169*, 19-26.

[40] Ahmad, N., Jaafar, M. S., Khan, S. A., Nasir, T., Ahmad, S., & Rahim, M. (2014). Measurement of radon exhalation rate, radium activity and annual effective dose from bricks and cement samples collected from Dera Ismail Khan. *American Journal of Applied Sciences*, *11*(2), 240.

[41] Williams, A. G., Zahorowski, W., Chambers, S., Griffiths, A., Hacker, J. M., Element, A., & Werczynski, S. (2011). The vertical distribution of radon in clear and cloudy daytime terrestrial boundary layers. *Journal of the atmospheric sciences*, *68*(1), 155-174.

[42] Raicharoen, T., Lursinsap, C., & Sanguanbhokai, P. (2003, May). Application of critical support vector machine to time series prediction. In *Proceedings of the 2003 International Symposium on Circuits and Systems, 2003. ISCAS'03.* (Vol. 5, pp. V-V). IEEE.

[43] Hipel, K. W., & McLeod, A. I. (1994). *Time series modelling of water resources and environmental systems*. Elsevier.

[44] Box, G. E., Jenkins, G. M., & Reinsel, G. (1970). Time series analysis: forecasting and control Holden-day San Francisco. *BoxTime Series Analysis: Forecasting and Control Holden Day1970*.

[45] Faraway, J., & Chatfield, C. (1998). Time series forecasting with neural networks: a comparative study using the airline data. *Journal of the Royal Statistical Society: Series C (Applied Statistics)*, *47*(2), 231-250.

[46] Amelin, M. (2013). Monte Carlo simulation in engineering. KTH Royal Institute of Technology, Electric Power Systems, Stockholm.

[47] http://people.brandeis.edu/~pmherb/MATLABbootcamp/montecarlo.html [Accessed: 12-Apr-2019].

[48] LeSage, J. P. (1999). Applied econometrics using MATLAB. *Manuscript, Dept. of Economics, University of Toronto*, 154-159.

[49] Xia, C., Wang, Q., Yu, T., Xu, G., & Yang, S. (2011). Variations of ionospheric total electron content before three strong earthquakes in the Qinghai-Tibet region. *Advances in space research*, *47*(3), 506-514.

[50] Boyarchuk, K., & Pulinets, S. (2005). *Ionospheric precursors of earthquakes*. Springer-Verlag Berlin Heidelberg.

[51] Harrison, R. G., Aplin, K. L., & Rycroft, M. J. (2014). Brief Communication: Earthquake–cloud coupling through the global atmospheric electric circuit. *Natural Hazards and Earth System Science*, *14*(4), 773-777.

[52] Harrison, R. G. (2014). Fair weather atmospheric electricity: its origin and applications. In *Proc. ESA Annual Meeting on Electrostatics* (p. 1).

[53] Harrison, R. G. (2013). The carnegie curve. *Surveys in Geophysics*, *34*(2), 209-232.

[54] Hirsikko, T., Laakso, L., Nieminen, S., Gagné, S., & Lehtipalo, K. (2011). Atmospheric ions and nucleation: a review of observations.

[55] Budden, K. G. (1988). *The propagation of radio waves: The theory of radio waves of low power in the ionosphere and magnetosphere*. Cambridge University Press.

[56] https://www.swpc.noaa.gov/phenomena/total-electron-content, [Accessed: 21-Mar-2019].

[57] Dobrovolsky, I. P., Zubkov, S. I., & Miachkin, V. I. (1979). Estimation of the size of earthquake preparation zones. *Pure and applied geophysics*, *117*(5), 1025-1044.

[58] Abumurad, K. M., & Al-Tamimi, M. (2001). Emanation power of radon and its concentration in soil and rocks. *Radiation measurements*, *34*(1-6), 423-426.

[59] Singh, B., Kushwah, V., Singh, O. P., Lakshmi, D. R., & Reddy, B. M. (2004). Ionospheric perturbations caused by some major earthquakes in India. *Physics and Chemistry of the Earth, Parts A/B/C*, *29*(4-9), 537-550.

[60] Jacobi, W., & Andre, K. (1963). The vertical distribution of radon 222, radon 220 and their decay products in the atmosphere. *Journal of Geophysical Research*, *68*(13), 3799-3814.

[61] Israel, H. (1973).Atmospheric Electricity Israel program for scientific translations. *Jerusalem*, *11*, 350.

[62] Volland, H. (Ed.). (1995). *Handbook of atmospheric electrodynamics* (Vol. 2). CRC Press.

[63] Pulinets, S. A., Khegaj, V. V., Boyarchuk, K. A., & Lomonosov, A. M. (1998). Atmospheric electric field as a source of ionospheric variability. *Uspekhi Fizicheskikh Nauk*, *168*(5), 582-589.

[64] Pulinets, S., & Boyarchuk, K. (2004). *Ionospheric precursors of earthquakes*. Springer Science & Business Media.

[65] Zhou, C., Liu, Y., Zhao, S., Liu, J., et.al. (2017). An electric field penetration model for seismo-ionospheric research. *Advances in Space Research*, *60*(10), 2217-2232.

[66] Engin, K. (2019). Isolation Entomopathogenic Fungi at Erzincan Province.

[67] "Population of provinces by years - 2000-2018". Turkish Statistical Institute. [Retrieved 9 March 2019].

[68] Avşar, Ü., Türkoğlu, E., Unsworth, M., Çağlar, İ., & Kaypak, B. (2013). Geophysical images of the North Anatolian Fault Zone in the Erzincan Basin, Eastern Turkey, and their tectonic implications. *Pure and Applied Geophysics*, *170*(3), 409-431.

[69] Rosie, A. Marc, D. et.al, (2003). Turkey, Rough Guides, ISBN 1-84353-071-6, p.1136, ISBN 978-1-84353-071-8, p.1016

[70] Gökalp, H. (2007). Local earthquake tomography of the Erzincan Basin and the surrounding area in Turkey. *Annals of Geophysics*.

[71] Okay, A. I. (2008). Geology of Turkey: a synopsis. *Anschnitt*, *21*, 19-42.

[72] Gürsoy, H., Tatar, O., Akpınar, Z., Polat, A., Mesci, L., & Tunçer, D. (2013). New observations on the 1939 Erzincan Earthquake surface rupture on the Kelkit Valley segment of the North Anatolian Fault Zone, Turkey. *Journal of Geodynamics*, *65*, 259-271.

[73] Akpınar, Z., Gürsoy, H., Tatar, O., Büyüksaraç, A., Koçbulut, F., & Piper, J. D. (2016). Geophysical analysis of fault geometry and volcanic activity in the Erzincan Basin, Central Turkey: Complex evolution of a mature pull-apart basin. *Journal of Asian Earth Sciences*, *116*, 97-114.

[74] Aydin, Ö. L., Bektaş, Ö., Büyüksaraç, A., & Yilmaz, H. (2019). 3D Modeling and Tectonic Interpretation of the Erzincan Basin (Turkey) using Potential Field Data. *Earth Sciences Research Journal*, *23*(1), 57-67.

[75] GEDİK, A. (2008). Geology of the Tertiary rocks around Kemah-Erzincan-Çayırlı region and their source rock characteristics. *Maden Tetkik ve Arama Dergisi*, *137*(137), 1-27.

[76] https://www.weather-tr.com/en/turkey/erzincan-climate, [Accessed: 25-Mar-2020].

APPENDICES

APPENDIX- 1: ARIMA AND MONTE-CARLO ON ERZINCAN RADON DATA

APPENDIX- 1: ARIMA AND MONTE-CARLO ON E 1

```
opts = spreadsheetImportOptions("NumVariables", 2);
% Specify sheet and range
opts.Sheet = "Sheet1";
opts.DataRange = "A2:B2002";
% Specify column names and types
opts.VariableNames = ["Date", "Rn222Bqm3"];
opts.VariableTypes = ["datetime", "double"];
% Import the data
tbl = readtable("C:\Users\MK\Desktop\peoples work\mustafa khairi\Radon Data.xlsx", opts,
"UseExcel")
Date = tbl.Date;
Radon = tbl.Rn222Bqm3;
Clear temporary variables
clear opts tbl
%load Radon data into your workspaace
Train=Radon(1:1900);%Getting training data
test=Radon(1900:2001);%test to test forecast
T = length(Radon);%this takes length of Radon data for plotting purposes
Plotting ACF and PACF of Train data to see how statonary it is, as well as the kind of
model to choose
%plotting ACF and PACF of the data
subplot(2,1,1)
autocorr(Train)%ACF of Radon Train data
subplot(2,1,2)
parcorr(Train)%PACF of Radon Train data
%we apply ARIMA(1,0,1)
model=arima(1,0,1)%declaring the model
Check Goodness of Fit Infer the residuals from the fitted model. Check that the residuals are
normally distributed and
uncorrelated
res = infer(fit,Train);%this is how to get the residual from the Train Radon data
% Plotting results
```

subplot(2,2,1)%subplots 2,2,1
plot(res./sqrt(fit.Variance))%plotting the standardized residuals
title('Standardized Residuals')%setting the title
subplot(2,2,2) %second plot
qqplot(res) %plotting the quantiles
subplot(2,2,3)
autocorr(res) %plotting autocorrelation function of the residual
subplot(2,2,4)
parcorr(res)%partial autocorrelation function of the residual
hvec = findall(gcf,'Type','axes');
set(hvec,'TitleFontSizeMultiplier',0.8,'LabelFontSizeMultiplier',0.8);%adjusting size and font
%The residual looks reasonable
% The residuals are reasonably normally distributed and uncorrelated.
Now Forecasting the results
Generate Forecasts Generate forecasts and approximate 95% forecast intervals for the next 100 or more time steps.
[yF,yMSE] = forecast(fit,100,'Y0',Train);%100 means path
UB = yF + 1.96*sqrt(yMSE); %this is just for upper bound
LB = yF - 1.96*sqrt(yMSE);%this is for lower forecast bound
%h4 = plot(Date(1:1900),Train,'green');%1:1900 means from begining to end of the train data
h4 = plot(Train,'blue');%1:4000 means from begining to end of the train data
hold on
h5 = plot(1901:2000,yF,'r','LineWidth',2);%1901:2000 from last train value to 100 points further
%h5 = plot(Date(1900:2000),yF,'r','LineWidth',2);%1900:2000 from last train value to 100 points further
%h6 = plot(Date(1900:2000),UB,'k--','LineWidth',1.5);%plotting upper bound for 100 further steps
h6 = plot(1901:2000,UB,'k--','LineWidth',1.5);%plotting upper bound for 100 further steps
plot(1901:2000,LB,'k--','LineWidth',1.5); %plotting the lower bound for 100
%plot(Date(1900:2000),LB,'k--','LineWidth',1.5); %plotting the lower bound for 100
legend([h4,h5,h6],'Radon','Forecast','Forecast Interval','Location','Northwest')%
title('Radon-training data 100 steps Forecast')%setting the title
axis tight
hold off
Now lets do the Monte-Carlo and simulate 5 paths and Forecast 100 time

steps

rng default % For reproducibility (I.e we can reproduce thesame result)

number_of_paths=7%number of Monte Carlo simulation Paths

number_of_paths = 7

%this below is the simulation code for Monte-Carlo(Please refer to Econometric tool box for details)

[Y E]=simulate(fit,100,'NumPaths',number_of_paths,'Y0',Train);

figure

subplot(2,1,1);

plot(1901:2000,Y)%here I plotted the 100 forecast steps from Last point of radon Train data

title('7 Simulated paths of Radon-Train data')

axis tight

Now lets plot The Radon data With ARIMA Monte-Carlo simulation forecast for 100 paths

rng('default')% For reproducibility (I.e we can reproduce thesame result)

[Ysim, E] = simulate(fit,100,'NumPaths',number_of_paths,'Y0',Train);%doing the monte Carlo again 100 steps

mn= mean(Ysim,2);%taking the mean simulation path

figure

plot(Train,'blue')%Now I am plotting the Normal Train Radon data

hold on

plot(1901:2000,Ysim);%Plotting 100 steps forecast.....(Note: there will be 7 curves because of simulation axis tight

h = plot(1901:2000,mn,'k--','LineWidth',2); %plotting the simulation Mean (i.e the mean of Monte-Carlo title('Simulated Radon-Paths') %setting title

legend(h,'Simulation Mean','Location','NorthWest')% legend

hold off6

Let's plot the Monte-carlo forecast with confidence Bounds

lower = prctile(Y,2.5,2);%lower bounds

upper = prctile(Y,97.5,2);%upper bounds

mn = mean(Y,2);%Monte carlo mean from the simulation path

figure

plot(1901:2000,test(1:100),'green')%here we are plotting the test but only 100 steps

legend("Radon test data")

axis tight

hold on

```
plot(1901:2000,lower,'r:','LineWidth',2);%plotting the lower bounds
axis tight
plot(1901:2000,mn,'k--','LineWidth',2);%Plotting the monte Carlo simulation mean
plot(1901:2000,upper,'r:','LineWidth',2)%plotting the upper bounds
axis tight
legend('radon test data','95% Interval','Simulation Mean','Location','best')
title('Radon data Forecast for 100 paths')
hold off
[yF,yMSE] = forecast(fit,100,'Y0',Train);%100 means path
UB = yF + 1.96*sqrt(yMSE); %this is just for upper bound
LB = yF - 1.96*sqrt(yMSE);%this is for lower forecast bound
h4 = plot(Train,'blue');%1:4000 means from begining to end of the train data
hold on
h5 = plot(1901:2000,yF,'r','LineWidth',2);%1901:2000 from last train value to 100 points further
h6 = plot(1901:2000,UB,'k--','LineWidth',1.5);%plotting upper bound for 100 further steps
h7=plot(1901:2000,test(1:100),'green')%here we are plotting the test but only 100 steps
h7 =
Line with properties:
Color: [0 1 0]
LineStyle: '-'
LineWidth: 0.5000
Marker: 'none'
MarkerSize: 6
MarkerFaceColor: 'none'
XData: [1×100 double]
YData: [1×100 double]
ZData: [1×0 double]
Show all properties
plot(1901:2000,LB,'k--','LineWidth',1.5); %plotting the lower bound for 100
legend([h4,h5,h6,h7],'Radon','Forecast','Forecast  Interval','test data','Location','Northwest')%
title('Radon-training data 100 steps Forecast')%setting the title
axis tight
hold off
rng('default')% For reproducibility (I.e we can reproduce thesame result)
```

```
[Ysim, E] = simulate(fit,100,'NumPaths',number_of_paths,'Y0',Train);%doing the monte Carlo again 100 steps
mn= mean(Ysim,2);%taking the mean simulation path
figure
plot(Train,'blue')%Now I am plotting the Normal Train Radon data
hold on
plot(1901:2000,Ysim);%Plotting 100 steps forecast.....(Note: there will be 7 curves because of simulation axis tight
h = plot(1901:2000,mn,'k--','LineWidth',2); %plotting the simulation Mean (i.e the mean of Monte-Carlo h2=plot(1901:2000,test(1:100),'green')%here we are plotting the test but only 100 steps
h2 =
Line with properties:
Color: [0 1 0]
LineStyle: '-'
LineWidth: 0.5000
Marker: 'none'
MarkerSize: 6
MarkerFaceColor: 'none'
XData: [1×100 double]
YData: [1×100 double]
ZData: [1×0 double]
Show all properties
title('Simulated Radon-Paths') %setting title
legend([h h2],'Simulation Mean','test','Location','NorthWest')% lege
```

CURRICULUM VITAE

Mustafa Khairi ARAB

PERSONAL INFORMATIONS

Birth of Place	: Duhok/ Iraq
Birth of Date	: 30/8/1990
Nationalty	: Iraq
Address	: Avro city/ Duhok
E-mail	: Mustafa.khairi90@gmail.com
Languages	: Arabic(Mother Tongue) English Excellent Speaking & Writing

EDUCATION

Bachelor	: Zakho University, Education Faculty, Department of Physics, Year 2011-2012
High School	: International School, Duhok City, Year 2007-2008

RESEARCH EXPERIENCES

- ✓ Computer Programming languages available (C++, MATLAB)
- ✓ Computer programs you can use (Microsoft Windows, Microsoft Office,)